Oceanic magmatism in sedimentary basins of the northern Gulf of California rift

Axel K. Schmitt[1,†], Arturo Martín[2], Bodo Weber[2], Daniel F. Stockli[3], Haibo Zou[4], and Chuan-Chou Shen[5]

[1]*Department of Earth and Space Sciences, University of California–Los Angeles, Los Angeles, California 90095-1567, USA*

[2]*Departamento de Geología, Centro de Investigación Científica y de Educación Superior de Ensenada (CICESE), Carretera Ensenada–Tijuana No. 3918, Zona Playitas, Ensenada, B.C., C.P. 22800, México*

[3]*Department of Geological Sciences, University of Texas at Austin, EPS RM 1.130, 1 University Station C9000, Austin, Texas 78712-0254, USA*

[4]*Department of Geology and Geography, Auburn University, 210 Petrie Hall, Auburn, Alabama 36849-5305, USA*

[5]*High-Precision Mass Spectrometry and Environment Change Laboratory (HISPEC), Department of Geosciences, National Taiwan University, Taipei 10617, Taiwan, R.O.C.*

ABSTRACT

Rift-related magmatism in the northernmost Gulf of California and the adjacent subaerial Salton Trough and Cerro Prieto basins comprises intermediate to rhyolitic surficial and buried lava flows and domes, including their xenolith cargo. In addition, geothermal drill wells frequently penetrate subsurface gabbroic to granitic sills and dikes, which intruded into Colorado River delta fluviatile and lacustrine sediments. Combined single-crystal U-Th-Pb and (U-Th)/He zircon ages reveal late Pleistocene to Holocene eruption ages for three volcanic centers in adjacent rift basins (from N to S): Salton Buttes (eruption age: 2.48 ± 0.47 ka; 95% confidence), Cerro Prieto (maximum eruption age: 73 ± 7 ka), and Roca Consag (eruption age: 43 ± 6 ka). U-Th zircon and allanite crystallization ages are close to the eruption ages, with the exception of Roca Consag lava, the zircon population of which is dominated by zircon with ca. 1 Ma crystallization ages, a population interpreted to be recycled from an unknown crustal source underlying the Wagner basin. Nd isotopic ratios for subsurface microgabbros from Cerro Prieto (ε_{Nd} = +8.9) overlap with values for mid-oceanic-ridge basalts (MORB) from the East Pacific Rise, adjacent to the southern Gulf of California. Cerro Prieto microgranites and Salton Sea basaltic xenoliths have similarly elevated ε_{Nd} values. The lowest ε_{Nd} value for late Pleistocene–Holocene igneous rocks from the northern Gulf of California is for Cerro Prieto dacitic lava (ε_{Nd} = +0.6). This value implies minor (<20%) assimilation of continental crustal rocks, which, however, is an upper limit because of crystal-scale evidence for magma contamination by unconsolidated sediment at the time of eruption. Zircon crystals in felsic rocks (rhyolite lavas, intrusive microgranites, and granophyre xenoliths) have trace-element and submantle $\delta^{18}O$ compositions that are robust indicators for a mafic source that has exchanged oxygen by interacting with meteoric hydrothermal fluids. Collectively, these data imply that oceanic rifting has initiated in the Salton Trough and Cerro Prieto basins. There, MORB-type magmas formed mafic intrusions within thick sedimentary basin fill, where they became exposed to deep-reaching hydrothermal fluids. Diverse intermediate- to high-silica rhyolitic magmas that are prevalent at the surface are produced by fractional crystallization of mafic parental magmas with minor assimilation of sediments or pre-rift basement rocks, and by partial melting of hydrothermally altered mafic intrusions.

INTRODUCTION

The southwestern North American continental margin evolved from a convergent plate boundary into a series of rift basins and embryonic oceanic spreading centers interconnected by NW-SE–oriented transform fault systems during the late Cenozoic (Lonsdale, 1989; Oskin and Stock, 2003). This plate boundary reconfiguration encompasses a transition between fundamentally different magma production mechanisms: during subduction, melting is triggered by hydration of the mantle wedge, whereas magmatism in continental rifts and divergent margins is due to decompression melting in the mantle, which ultimately produces compositionally uniform, nearly anhydrous mid-ocean-ridge basalts (MORB). First-order compositional differences often result from the transition between these two magmatic regimes, where subduction is associated with predominantly intermediate compositions, whereas bimodal suites are a hallmark of continental rifting (e.g., Bryan and Ernst, 2008). During incipient rifting, the proximity to sources of continent-derived detritus shed into rift basins can also exert strong control on the compositional diversity of magmas and their representation in the geological record. These controls include (1) density filtering of magmas where negatively buoyant mafic magmas stall within sequences of low-density sediments so that the record of surficial volcanic rocks is not representative of magma flux at depth (e.g., Fuis et al., 1984); (2) rapid subsidence and burial, which conceal earlier phases of magmatism (e.g., Herzig, 1990; Hurtado-Brito, 2012); (3) contamination of magmas during ascent through thick sequences of sedimentary basin fill (through melting and assimilation, or mingling between magma and sediment; e.g., Gibson et al., 1997); and (4) metamorphism and hydrothermal alteration caused by fluid circulation through porous sediments in magmatically active rift zones (e.g., Einsele et al., 1980; McKibben et al., 1988).

In order to better constrain the origins of rift-related magmatism and the interaction between magma and sediment during continental breakup, we studied a comprehensive suite of surface and subsurface magmatic rocks from the northern Gulf of California, consisting of samples from two subaerial rift basins (Salton Trough, Cerro Prieto) and the submarine

†E-mail: axelk@argon.ess.ucla.edu

GSA Bulletin; November/December 2013; v. 125; no. 11/12; p. 1833–1850; doi: 10.1130/B30787.1; 14 figures; 3 tables; Data Repository item 2013358.

Wagner basin (Fig. 1). In addition to whole-rock geochemical analysis, we also focused on single-crystal geochemical and geochronological analysis of zircon as a robust indicator mineral. Single-crystal zircon geochronology permits us to constrain magmatic crystallization and eruption ages at high temporal resolution, even for subsurface rocks highly altered by geothermal activity. Alteration-resistant geochemical indicators such as whole-rock Nd isotopes and zircon oxygen isotopes indicate dominantly MORB-type magma sources for parental magmas, with remelting of hydrothermally altered juvenile mafic crust as an important mechanism to produce high-silica magma compositions. Thick sedimentary rift basin infill controls magma ascent and biases extrusive magmatism toward silicic compositions, but melting of sediment or prerift basement overall contributes negligibly to even the most silicic magma compositions.

GEOLOGICAL BACKGROUND

Mid-Miocene to Holocene Magmatic Evolution

Baja California and western Sonora are well-known examples of diverse, and in part unusual postconvergent magma compositions (e.g., Till et al., 2009; Calmus et al., 2011). These are predated by an earlier phase of arc volcanism related to the terminal phase of subduction of Farallon plate fragments (20–12 Ma). Subduction-related rocks are widespread along the entire eastern margin of the Baja California peninsula (Fig. 1). They are termed Comondú volcanic group in the southern half of the peninsula (e.g., Hausback, 1984; Sawlan, 1991; Umhoefer et al., 2001), with equivalent rocks also preserved in the northern half (Martín et al., 2000). After cessation of subduction, postsubduction basaltic fissure eruptions (e.g., Bellon et al., 2006; Benoit et al., 2002) and peralkaline silicic ignimbrite volcanism initiated after ca. 12 Ma and lasted until ca. 8 Ma (Mora-Klepeis and McDowell, 2004; Oskin and Stock, 2003; Vidal-Solano et al., 2008). These silicic rocks are mostly exposed in northwestern mainland Mexico, but remnants of pyroclastic flow deposits are locally preserved along the eastern margin of Baja California (Ferrari et al., 1999; Oskin and Stock, 2003). Contemporaneous with an initial phase of marine incursion into the proto–Gulf of California, dominantly bimodal volcanism persisted between ca. 8 and 3 Ma, for example, in the Puertecitos volcanic field (Fig. 1; Martín-Barajas et al., 1995).

Post–3 Ma magmas in the southern Gulf of California are largely tholeiitic basalts, and their

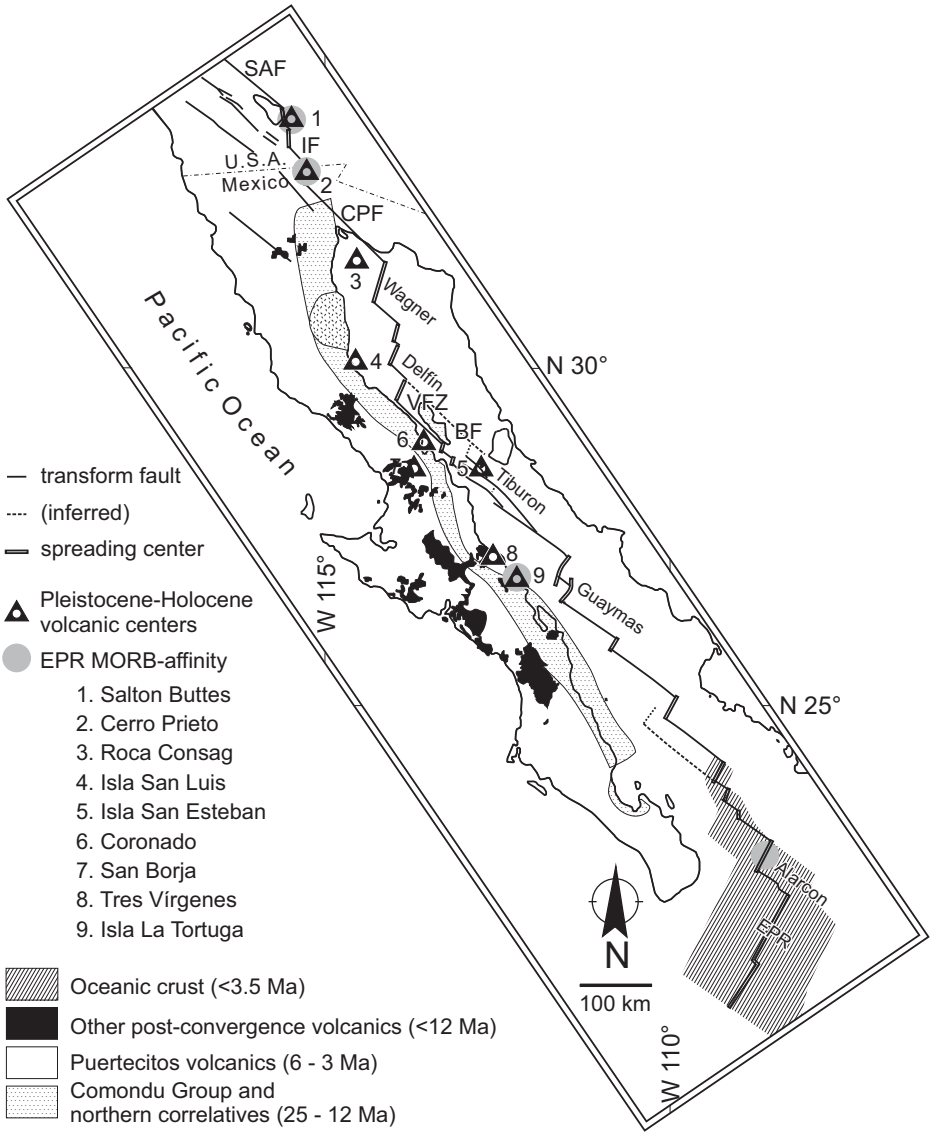

Figure 1. Distribution of subduction and postsubduction volcanism in Baja California and the Gulf of California (after Schmitt et al., 2006). Solid lines show major faults related to NW-SE translation between the Pacific and North American plates (after Lonsdale, 1989): SAF—San Andreas fault, IF—Imperial fault; CPF—Cerro Prieto fault; VFZ—Volcanes fault zone; BF—Ballenas fault. Locations of major rift basins are indicated. EPR—East Pacific Rise; MORB—mid-ocean-ridge basalt.

associated vents are confined to the axes of en-echelon basins separated by NW-SE–trending right-lateral transform faults (e.g., Batiza, 1978; González-Escobar et al., 2009, 2010). Toward the mouth of the Gulf of California, there is clear evidence from magnetic striping for seafloor spreading (Lonsdale, 1989), whereas to the north the basins are blanketed by thick deposits of continental detritus, which prohibit geomagnetic verification of oceanic spreading. Seismic-reflection data (Martín et al., 2013), however, indicate ~40–60-km-wide, newly formed oceanic crust in the Tiburón, Delfín, and Wagner basins. Numerous magmatic intrusives, volcanic edifices, and their pyroclastic deposits have been seismically imaged within the Upper and Lower Delfin basins, and several volcanic edifices exist along the Ballenas transform fault and the Volcanes fault zone along the edge of the Baja California continental crust (Fig. 1; Persaud et al., 2003; Hurtado-Brito, 2012). Isolated late Pleistocene to recent volcanic centers are also scattered outside the basins along the eastern coast of Baja California: Tres Vírgenes (Capra et al., 1998; Schmitt et al., 2006, 2010); Isla San Luis (Paz-Moreno and Demant, 1999);

and within the Ballenas Channel (Martín-Barajas et al., 2008).

Of the three northernmost basins in the Gulf of California, the Salton Trough and Cerro Prieto basins are subaerial due to their proximity to the Colorado River delta. The origin of these basins has long been interpreted to be analogous to the fully oceanic basins farther south in the Gulf of California (Elders et al., 1972). The Wagner and Consag basins adjacent to the south are submarine, albeit with average water depths that are much shallower than in the central and southern Gulf of California. Although surficially emplaced basalt is absent in the subaerial basins, mafic intrusions are demonstrably abundant at depth based on drill well penetration, and their existence is also evident from xenolith populations, and from the geochemical characteristics of consanguineous felsic lavas (see later herein).

A particular puzzling phenomenon is the persistence, and in some locations re-initiation, of magmatism with subduction-type chemical affinities along strike of the Gulf of California rift (Bigioggero et al., 1995; Martín-Barajas et al., 1995; Capra et al., 1998; Negrete-Aranda and Canon-Tapia, 2008). Within the northernmost Gulf of California rift system (Fig. 2), such diverse compositional types of volcanism exist side-by-side to the present day: In the Salton Trough, a prominent silicic gap exists between basaltic and rhyolitic end members, whereas silicic to intermediate magma compositions dominate the adjacent Cerro Prieto basin (Figs. 3 and 4). Multiple models for this wide spectrum of postconvergent magmatism in the Gulf of California have been proposed: subduction metasomatism enhancing mantle fertility combined with thermal insulation of the mantle by thick sediments (Lizarralde et al., 2007), melting of slab remnants (Aguillon-Robles et al., 2001) or lower-crustal metabasites (Castillo, 2008), variable degrees of peridotite melting (Robinson et al., 1976), fractional crystallization of basaltic magma (Herzig, 1990; Herzig and Jacobs, 1994), partial melting of granitic basement (Reed et al., 1984), assimilation of continental crust concomitant with crystal fractionation (Martín-Barajas and Weber, 2003; Vidal-Solano et al., 2008), and partial melting of hydrothermally altered basaltic crust (Schmitt and Vazquez, 2006).

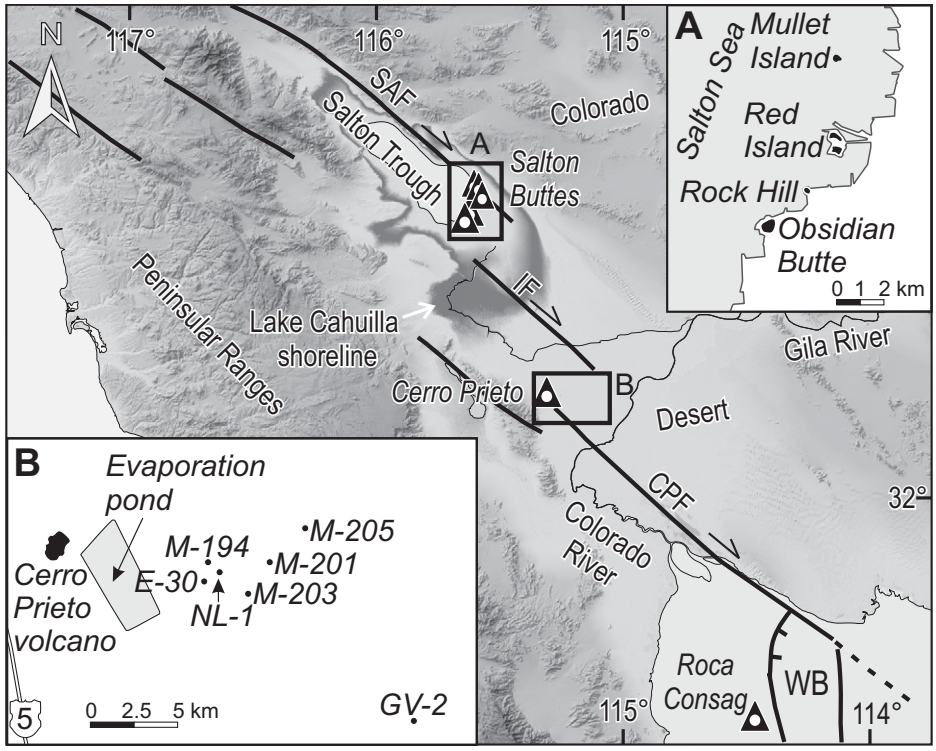

Figure 2. Geological overview map of the northern Gulf of California with locations for surface volcanoes. On-land depressions below sea level are indicated by gray shading; solid lines indicate major faults (see Fig. 1 for abbreviations). Insets show locations of lava domes and sampled geothermal wells for the (A) Salton Sea and (B) Cerro Prieto geothermal fields. WB—Wagner basin.

Recent Volcanism in the Salton Trough, Cerro Prieto, and Wagner Basins

In the Salton Trough, the series of five rhyolite domes (from NE to SW: Mullet Island, two domes of Red Island, Rock Hill, and Obsidian Butte) is collectively termed the Salton Buttes (Fig. 2). Early pyroclastic deposits overlying lacustrine sediments of Pleistocene–Holocene Lake Cahuilla are covered by lava flows and domes up to 40 m thick, but their elevations are entirely below sea level. Domes show wave-cut benches, and rounded pumice rafts are present at paleoshorelines, suggesting eruption prior to or during a highstand of Lake Cahuilla, the natural precursor of the Salton Sea. Because all five domes are petrologically similar and occur on a single N-S–trending lineament, they are likely connected by a common feeder dike (Kelley and Soske, 1936; Robinson et al., 1976). Salton Buttes rhyolite lavas are crystal poor, with only minor plagioclase phenocrysts present. They contain, however, a diverse assemblage of xenoliths of basalt, granite, and metasediment (Kelley and Soske, 1936; Robinson et al., 1976; Schmitt and Vazquez, 2006). Basaltic xenoliths have depleted trace-element signatures and elevated ε_{Nd} ($^{143}Nd/^{144}Nd$) coupled with low $^{87}Sr/^{86}Sr$, characteristic of an East Pacific Rise mantle source (Herzig and Jacobs, 1994; Robinson et al., 1976). The granitic xenoliths are derived from juvenile crust rather than basement and originated from remelting of hydrated mafic crust (Schmitt and Vazquez, 2006). This is supported by the presence of rhyolitic glass, representing partial melt in the basaltic xenoliths (Robinson et al., 1976).

Cerro Prieto basin contains only one volcano (Fig. 2), a composite lava dome that rises to 223 m above sea level and is surrounded by peripheral autobrecciated lava injections into unconsolidated Colorado River deltaic sediments. The dacitic lava is fine grained and crystal poor, with rare plagioclase phenocrysts present. Rounded xenoliths of indurated and baked sediments are locally enclosed in the autobrecciated lava.

Roca Consag (Fig. 2) is an isolated volcanic plug located near the SW terminus of the submarine Wagner basin (González-Escobar et al., 2010). It consists of microphyric low-K dacite, and likely subvolcanic intrusive rock. Its spatial extent is ~0.002 km^2, and its elevation is ~40 m above sea level.

Previous radiometric dating for the Salton Buttes and Cerro Prieto resulted in mostly K-Ar ages. For Salton Buttes obsidian, ages range from 33 ± 36 ka to <10 ka. Late Pleistocene to Holocene U-Th zircon crystallization ages exist for Salton Buttes obsidian and xenoliths

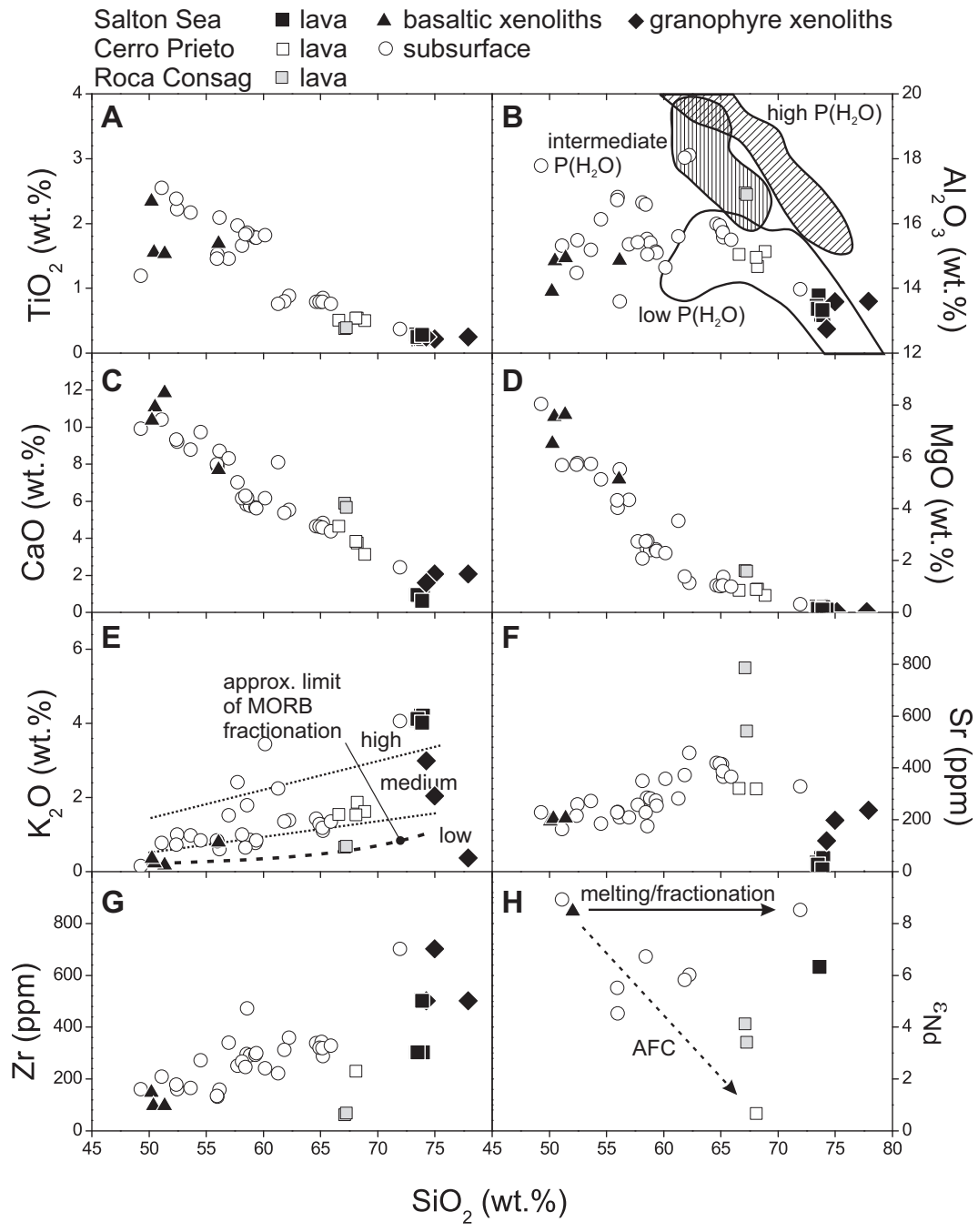

Figure 3. Major- and trace-element variation diagrams for northern Gulf of California igneous rocks. Panel B shows compositional fields for melting of hydrous basaltic rocks under different water pressures (Thy et al., 1990). Thick dashed line in panel E is the limit of K_2O enrichment from closed-system mid-ocean-ridge basalt (MORB) fractionation (France et al., 2010). Solid and dashed arrows in panel H schematically indicate compositional trends for closed-system remelting, and fractional crystallization coupled with assimilation of continental crustal material (AFC), respectively. Data sources: this study, and compiled from Robinson et al. (1976), Reed et al. (1984), Herzig and Elders (1988), and Herzig (1990).

(Schmitt and Vazquez, 2006). Obsidian hydration methods yielded surface exposure age estimates between ca. 8.4 ka and ca. 2.5 ka (Friedman and Obradovich, 1981; cf. Anovitz et al., 1999). Recently published (U-Th)/He zircon ages for a granophyre xenolith indicate an eruption age for Red Island of 2.48 ± 0.47 ka (Schmitt et al., 2013). Two groundmass K-Ar analyses for Cerro Prieto are comparatively imprecise at 100 ± 60 ka and 120 ± 70 ka (Reed et al., 1984), with no radiometric ages available for Roca Consag prior to this study.

Subsurface Magmatism

Earlier volcanic episodes in the northern Gulf of California rift basins are largely obscured due to rapid subsidence and sedimentation. However, geothermal drill wells have frequently penetrated igneous rocks at various depths in the subsurface, suggesting long-lived and widespread magmatic activity. Subsurface igneous rocks are frequently hydrothermally altered and resided at reservoir temperatures of up to 390 °C (Schmitt and Hulen, 2008). For the Salton Trough, U-Pb zircon ages for lava flows and pyroclastic deposits (including distal Bishop Ash) that are present at depths of ~1.7–2.2 km range between ca. 420 ka and 760 ka, yielding subsidence and sedimentation rates of ~2–4 mm/yr (Schmitt and Hulen, 2008). At depth, these Pleistocene sediments are presently undergoing prograde metamorphism, with neoblastic biotite and garnet indicating temperatures >350 °C (McDowell and Elders, 1980). Seismically, this zone of metamorphosed sediments is identified as an ~10-km-thick

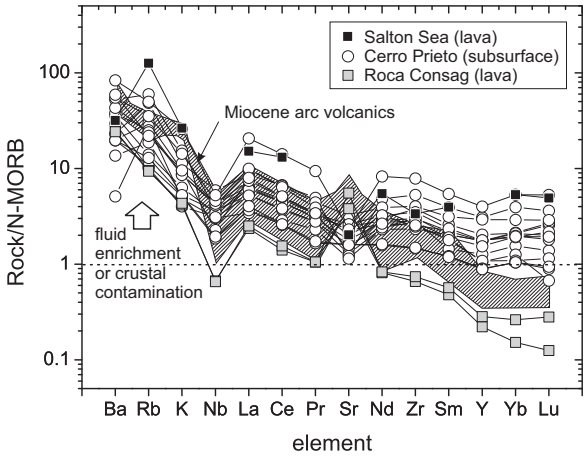

Figure 4. Spidergrams for late Pleistocene mafic and intermediate rocks from Cerro Prieto and Roca Consag normalized to mid-ocean-ridge basalt (N-MORB; Niu et al., 1999). Fluid-compatible trace elements are plotted on left. Miocene subduction-related intermediate volcanic rocks from northeastern Baja California (Martín et al., 2000) plotted for comparison show similar enrichments, despite the absence of ongoing subduction. Note that subduction-related addition of incompatible elements and contamination with continental crustal rocks lead to largely indistinguishable trace-element patterns. Data sources: this study, except Salton Buttes lava data, which are from Herzig and Elders (1988).

high-velocity section that also could contain an unknown volume of mafic intrusive rocks (Fuis et al., 1984). Gravity and magnetic anomalies in the Salton Trough have also been interpreted as recording the presence of shallow mafic intrusions (Kasameyer and Hearst, 1988).

From the geothermal operator at Cerro Prieto (Comisión Federal de Electricidad [CFE]), we obtained well cuttings identified by core loggers as igneous rocks that were penetrated in several geothermal wells (Fig. 5). In total, ~100 cutting samples from seven wells (E-30, M-194, NL-1, GV-2, M-201, M-203, M-205), each sample consisting of ~50–100 g of millimeter-sized fragments sampled at 1 m intervals, were petrographically investigated using a binocular microscope, petrographic microscope, and scanning electron microscope (SEM).

In these wells, the shallow sections (to ~1.5 km depth in the SW and ~2.5 km in the NE) are composed of unconsolidated sediments, whereas deeper sections are dominantly shale and quartzite. Igneous samples comprise volcanic rocks at shallow levels (e.g., NL-1 1494 m; M-203 1608 m) with thicknesses of ~20 m (Fig. 5). These volcanic rocks are aphyric, glassy, and vesiculated, and they represent buried pyroclastic fallout deposits. At greater depth, igneous rocks appear to be sill-like intrusions based on similar depths of intersection in neighboring wells (e.g., microgranites at ~3000 m in E-30 and NL-1). These intrusions are up to ~40 m in thickness, although exact determination is compromised by mixing between cuttings derived from different depth intervals. Mafic intrusives are fine-grained gabbroic rocks, with plagioclase and clinopyroxene as the dominant phenocrysts with ophitic texture and a brownish glassy to microcrystalline groundmass (e.g., E-30 3048 m; E-30 3069 m; M-201 3534 m; M-205 2579 m). Intrusive intermediate rocks are dominated by plagioclase with a trachytic texture (e.g., M-203 3921 m; M-203 3954 m). Felsic intrusive rocks are leucocratic microgranites with plagioclase microphenocrysts surrounded by granophyric intergrowths of quartz and alkali-feldspar (e.g., E-30 3027 m). Opaque minerals, and in some cases sulfides (sphalerite), zircon, and allanite, are present as accessory minerals (e.g., NL-1 3129 m). Remarkably, gabbroic, intermediate, and felsic intrusive rocks occur in close spatial proximity within an ~20 m depth interval in some wells (e.g., between 3027 and 3048 m in well E-30; Fig. 5).

METHODS

Sampling

For accessory mineral geochronology and geochemistry (trace elements and oxygen isotopes), lava from Cerro Prieto and Roca Consag was sampled to complement published data for the Salton Buttes surface and subsurface rocks (Schmitt and Vazquez, 2006; Schmitt and Hulen, 2008; Schmitt et al., 2013). We also extracted zircon from Cerro Prieto well cuttings, but only two felsic intrusives yielded juvenile zircon. Because of the requirement to process comparatively large amounts of samples (tens of grams) for heavy mineral separation, we acknowledge contamination of the cuttings by overlying wall rock in the wells. Whole-rock geochemical data (including Th, Sr, and Nd isotopes) were obtained from samples where literature data were unavailable or incomplete. For whole-rock geochemical analysis of cuttings, a gram-sized aliquot of magmatic fragments was handpicked under a binocular microscope, and thus contamination by wall-rock fragments can be ruled out. For comparison, published whole-rock compositional and isotopic data were compiled (Robinson et al., 1976; Herzig, 1990; Herzig and Jacobs, 1994; Schmitt and Hulen, 2008).

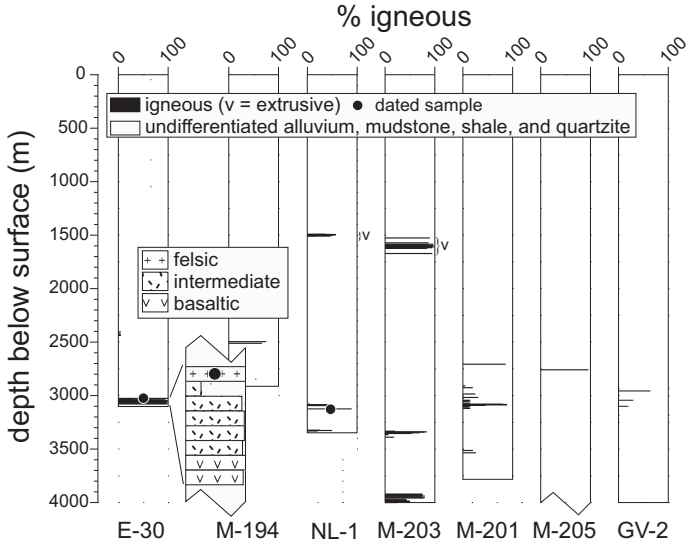

Figure 5. Simplified well logs showing distribution of igneous rocks in Cerro Prieto geothermal wells. Percentages of igneous cuttings per 3 m depth interval were visually estimated under a binocular microscope.

Geochronology

U-Th and U-Pb Zircon

Zircon crystals for U-Th and U-Pb dating (Tables DR1 and DR2[1]) were density separated from crushed rocks using heavy liquids. Clear and euhedral zircon crystals were subsequently handpicked, placed with a prism face onto a flat indium (In) metal surface, and pressed into the In using a flat tungsten carbide metal anvil and an arbor press. The In-mounted zircon crystals were ultrasonically cleaned in 1 *N* HCl and deionized water, and then coated with a gold layer, several tens of nanometers thick, to provide a conductive surface. Analysis spots on unsectioned crystals are identified as "rim," whereas "interior" refers to crystals analyzed after sectioning and polishing to tens of micrometers using abrasives. For samples with too little material available for heavy mineral separation (e.g., NL-1), thin sections of cuttings were screened by SEM, and the interiors of accessory zircon and allanite were analyzed in situ.

Isotopic analysis was conducted by secondary ion mass spectrometry (SIMS) using the CAMECA IMS 1270 at the University of California–Los Angeles (UCLA; techniques modified from Reid et al., 1997; Schmitt et al., 2006; Vazquez and Reid, 2004). The main differences to previously published methods are crystal rim analysis to ~5 µm depths at lateral beam diameters of ~25–35 µm, and the use of dual electron multipliers separated by two atomic mass units in order to simultaneously collect background intensities at mass/charge ~244 and $^{230}Th^{16}O^+$ at mass/charge ~246. Dual collection reduces the magnet cycling time by ~20%. Primary beam currents ($^{16}O^-$) were 40–60 nA, and total analysis duration per spot was 25 min. Zircon standard AS3 was used for Th/U relative sensitivity calibration and as an equilibrium zircon standard for which (^{230}Th)/(^{238}U) = 1.008 ± 0.007 (mean square of weighted deviates [MSWD] = 0.51; n = 33) was obtained on analyses interspersed with the unknowns. Zircon elemental concentrations were calculated from $^{238}U^{16}O^+/^{90}Zr_2{}^{16}O_4^+$ intensity ratios calibrated on zircon standard 91500 with U = 81.2 ppm (Wiedenbeck et al., 2004).

U-Pb zircon analyses were conducted using the CAMECA IMS 1270 at UCLA following techniques outlined in Grove et al. (2003) and Schmitt et al. (2003). Zircons were handpicked from heavy-liquid mineral separates, embedded in epoxy, and polished to expose crystal interiors. A 20 nA primary beam was focused onto a spot with ~15 µm diameter. Secondary ion intensities were acquired in 10 magnet cycles per analysis, resulting in a crater depth of ~1 µm. Throughout the manuscript, we report and plot individual data points with 1σ errors, but we state average age uncertainties at 95% confidence. Half-lives and isotopic ratios are from Jaffey et al. (1971) and Cheng et al. (2000).

(U-Th)/He Zircon

The (U-Th)/He age determinations were carried out at the University of Kansas using laboratory procedures described in Biswas et al. (2007). In cases where unsectioned crystals where analyzed by SIMS, zircons were extracted from the mounts using a steel picking needle. Individual crystals were wrapped in Pt foil, heated for 10 min at 1290 °C, and reheated until >99% of the He was extracted from the crystal. All ages were calculated using standard α-ejection corrections using morphometric analyses (Table 1; Farley et al., 1996). After laser heating, zircons were unwrapped from the Pt foil and dissolved using double-step HF-HNO_3 and HCl pressure-vessel digestion procedures (Krogh, 1973). U, Th, and Sm concentrations were determined by isotope dilution–inductively coupled plasma–mass spectrometry (ID-ICP-MS) analysis. The laboratory routinely analyzes zircon standards with independently determined ages, and we report averages for Fish Canyon tuff zircons of 27.8 ± 0.1 Ma (1 relative standard deviation RSD% = 4%; n = 285). Reported age uncertainties reflect the reproducibility of replicate analyses of these laboratory standard samples (Farley et al., 2002), but for much younger zircons such as the ones analyzed here, analytical uncertainties are significantly larger. We accounted for these by multiplying the average age uncertainty by the square-root of the MSWD.

Compositional and Isotopic Analysis

Major and Trace Elements in Whole Rocks and Zircon

Whole-rock compositional analysis of lava samples was conducted using X-ray fluorescence (XRF) and ICP-MS analysis at University of Washington (Table 2). For cuttings from geothermal well samples, major and trace elements were analyzed in bulk using electron microprobe analysis (EMPA) and SIMS, respectively, by the fused-bead method (Table 2; Nicholls, 1974). Fused-bead analysis minimizes sample consumption, and aids in avoiding contamination by sedimentary rocks in the well cuttings because only small amounts of handpicked igneous fragments are required. These were ground in an agate mortar, and the majority of powder was retained for Sr and Nd isotopic analysis. Only ~100 mg samples of rock powder were fused into millimeter-sized glass beads using an electrically heated tungsten crucible in an Ar atmosphere. The glass beads typically contained ~1–4 wt% of WO_3 from the crucible material, and all data are reported normalized to 100% W-free. XRF and glass bead EMPA major elements for Cerro Prieto sample CP05–2 agree within ±5%, except for FeO and Na_2O, which are ~6% and ~10% lower in the fused beads compared to XRF values. Trace-element analyses of glasses and zircons (Table DR3 [see footnote 1]) were conducted by SIMS using energy-filtering to suppress molecular interferences modified from the procedure in Monteleone et al. (2007). NIST SRM610 glass was used as a primary standard (Pearce et al., 1997), and accuracy was monitored by analysis of BHVO-2 glass and 91500 zircon. For most trace elements (in particular rare earth elements [REEs] + Y), SIMS abundances for BHVO-2 (whole rock) and 91500 (zircon) agree within ±12% with published values (Wilson, 1997; Liu et al., 2010).

Oxygen Isotopes in Zircon

Oxygen isotopes in zircon (Table DR4 [see footnote 1]) were analyzed by SIMS using multicollection dual Faraday cup analysis as described in Trail et al. (2007). Unknowns were bracketed by analysis of AS3 standard zircon with $\delta^{18}O$ = 5.34‰ (Trail et al., 2007), and accuracy was estimated by analyzing 91500 zircon as a secondary standard ($\delta^{18}O$ = 9.98‰; Wiedenbeck et al., 2004), which was mounted in the same geometry as the unknowns. The deviation from the published value for 91500 is ~0.2‰, commensurate with the SIMS reproducibility of the primary standard AS3.

U-Th Isotopes in Whole Rocks

U and Th were separated using ion-exchange column methods described in Shen et al. (2003). Isotopic measurements were conducted on a Thermo Electron Neptune multicollector (MC) ICP-MS at the High-Precision Mass Spectrometry and Environment Change Laboratory (HISPEC), Department of Geosciences, National Taiwan University (Shen et al., 2012). A triple-spike, ^{229}Th-^{233}U-^{236}U, isotope-dilution method was employed to correct mass bias and determine uranium concentration (Shen et al., 2002). Uncertainties in concentration and isotopic data include corrections for blanks, instrumental fractionation, multiplier dark noise, spectral interferences, and errors associated with quantifying the isotope composition in the spike solution (Table 3).

[1]GSA Data Repository item 2013358, Table DR1 (U-Th zircon geochronology), Table DR2 (U-Pb zircon geochronology), Table DR3 (zircon trace elements), and Table DR4 (zircon oxygen isotopes), is available at http://www.geosociety.org/pubs/ft2013.htm or by request to editing@geosociety.org.

TABLE 1. SUMMARY OF (U-Th)/He AND U-Th ZIRCON GEOCHRONOLOGY

Sample-grain	Age (ka)	± (ka)	U (ppm)	Th (ppm)	Th/U	^{4}He (nmol/g)	Mass (μg)	Ft†
Cerro Prieto lava (32°25′26″N, 115°18′3″W)								
CP09-04-1	14400	1200	196	279	1.42	16.4	10.7	0.81
CP09-04-2	98700	7900	201	137	0.683	97.7	6.9	0.78
CP09-04-4	87700	7000	322	227	0.705	132	3.9	0.74
CP09-04-5	5900	500	613	1282	2.09	20.9	3.5	0.71
CP09-04-6	117100	9400	141	47	0.334	71.7	3.9	0.74
CP09-04-9*	68.4	5.5	227	59	0.259	0.073	12.2	0.82
CP09-04-10	105000	8400	497	213	0.429	235	4.5	0.75
CP09-04-11	22000	1800	288	174	0.605	27.3	2.2	0.70
CP09-04-13	172	14	224	84	0.375	0.171	5.3	0.76
CP09-04-14	86600	6900	113	71	0.625	47.1	5.9	0.77
CP09-04-M1	533600	42700	76.7	40.8	0.531	188	9.3	0.73
CP09-04-M2	415800	33300	10.8	4.7	0.434	23.6	73.9	0.86
Cerro Prieto sedimentary enclave (32°25′21″N, 115°18′45″W)								
CP0702D-1	901	72	207	85	0.410	0.818	4.2	0.74
CP0702D-2	26400	2100	344	107	0.311	39.4	4.5	0.75
CP0702D-3	389	31	35.8	20.5	0.573	0.067	8.0	0.78
CP0702D-4	8400	700	543	409	0.753	20.9	3.4	0.72
CP0702D-5*	78.0	6.2	193	132	0.683	0.064	2.1	0.67
CP0702Dr-1	5800	500	144	19	0.135	3.67	6.6	0.79
CP0702Dr-2	3500	300	140	26	0.188	2.08	4.0	0.76
CP0702Dr-3	2200	200	258	32	0.123	2.38	3.5	0.74
CP0702Dr-4	3300	300	64.3	50.6	0.787	1.01	3.3	0.73
CP0702Dr-5	15700	1300	136	41	0.297	9.32	4.4	0.76
Average age: 73 ± 7 ka (n = 2)								
Roca Consag lava (31°6′45″N, 114°29′17″W)								
RC01-24A-1	75.1	6.0	161	263	8.55	1.64	2.2	0.62
RC01-24A-2*	53.1	4.3	80.3	38.9	2.08	0.485	6.2	0.78
RC01-24A-3*	53.1	4.2	176	107	3.47	0.609	4.4	0.72
RC01-24A-4*	36.4	2.9	60.2	30.2	2.76	0.503	3.4	0.73
RC01-24A-5*	59.8	4.8	95.7	35.4	2.22	0.370	5.3	0.75
RC01-24A-6*	42.5	3.4	280	132	6.33	0.469	3.9	0.73
RC01-24A-7*	54.5	4.4	500	301	6.41	0.602	4.4	0.75
RC01-24A-8*	30.8	2.5	233	46	0.990	0.198	8.3	0.79
RC01-24A-9*	50.2	4.0	71.7	29.8	1.82	0.415	5.8	0.77
RC01-24A-10*	51.7	4.1	185	54	2.47	0.290	7.6	0.78
RC01-24A-11*	41.6	3.3	39.6	17.7	1.42	0.447	6.6	0.78
RC01-24A-12*	38.0	3.0	208	103	1.33	0.495	4.4	0.76
Average age: 43 ± 6 ka (n = 11; mean square of weighted deviates [MSWD] = 7.1)								

*Used for average.
†Ft—correction factor for ^{4}He ejection errors 1σ.

Sr-Nd Isotopes in Whole Rock

Sample preparation and element separation for Sr and Nd isotope analyses were carried out in PicoTrace® clean laboratory facilities at Centro de Investigación Científica y de Educación Superior de Ensenada (CICESE), Ensenada, Mexico. Approximately 100 mg aliquots of handpicked and powdered whole rock were heated at 165 °C for 15 h in a mixture of ~3–4 mL double-distilled concentrated HF, ~1 mL double-distilled concentrated HNO_3, and a few drops of distilled concentrated $HClO_4$ using a PicoTrace DAS® pressure digestion system. After evaporation, the residues were dissolved in 2 *N* HCl. Strontium and REEs were separated using quartz glass columns filled with Dowex AG50-WX8 cation-exchange resin in HCl medium. Sm and Nd were separated in quartz-glass columns filled with LN-Spec® resin in HCl medium.

Neodymium isotope ratios were measured at Laboratorio Universitario de Geoquimica Isotopica (LUGIS), Instituto de Geofísica, Universidad Nacional Autónoma de México, using a Finnigan MAT 262 thermal ionization mass spectrometer (TIMS) equipped with eight variable collectors and one fixed Faraday collector in static mode. Strontium isotope compositions were measured either at LUGIS or at Scripps Institution of Oceanography, La Jolla, California, using a nine-collector, Micromass Sector 54 TIMS. Isotopic ratios were corrected for mass fractionation by normalizing to $^{86}Sr/^{88}Sr$ = 0.1194 and $^{146}Nd/^{144}Nd$ = 0.7219. Neodymium isotopes are reported relative to $^{143}Nd/^{144}Nd$ = 0.51185 for the La Jolla Nd standard, and Sr isotopes are reported relative to NBS 987 $^{87}Sr/^{86}Sr$ = 0.71025. Because of the young age of the samples, no age corrections were applied, and elemental abundances are from XRF and SIMS whole-rock analyses (Table 2).

GEOCHRONOLOGY RESULTS

Salton Buttes

The best evidence for the youthfulness of the Salton Buttes is from published (U-Th)/He zircon ages for Red Island granophyre xenolith (Fig. 6), as well as U-Th zircon crystallization ages from rhyolite lavas and the granophyre xenolith (Fig. 7; data from Schmitt and Vazquez, 2006; Schmitt et al., 2013). The Red Island (U-Th)/He zircon eruption age is 2.48 ± 0.47 ka (Schmitt et al., 2013). In the $^{230}Th/^{232}Th$ versus $^{238}U/^{232}Th$ activity diagram, Salton Buttes zircon compositions fall in a wedge-shaped field ("sphenochron"), with the low U-Th apex of this wedge pointing toward the whole-rock composition (Figs. 7A and 7B; Schmitt and Vazquez, 2006; Schmitt et al., 2013). This indicates that the duration of zircon crystallization was protracted relative to the half-life of ^{230}Th. U-Th zircon–whole rock model ages date back to ca. 20 ka in the lavas, and ca. 40 ka in the granophyre xenolith, with the youngest crystals and crystal populations yielding ages of 5.5 ± 1.2 ka and 2.9 ± 0.6 ka, respectively (Figs. 7A and 7B). The onset of crystallization therefore must have preceded the eruption by at least several tens of thousands of years, but zircon likely continued to crystallize until shortly before eruption.

Cerro Prieto

An extensive search for zircon in Cerro Prieto by processing ~20 kg of rock yielded only scarce (~20) mostly small, rounded, and brownish zircon crystals in the heavy mineral fraction. Only three clear, needle-shaped zircon crystals were found, but these were too small for (U-Th)/He analysis because long stopping distances of alpha particles result in significant loss of radiogenic ^{4}He (Farley et al., 1996). U-Th and U-Pb dating confirmed that most brownish Cerro Prieto zircons are xenocrystic with ages between ca. 60 Ma and ca. 2 Ga (Fig. 8A; Tables DR1 and DR2 [see footnote 1]), whereas the clear crystals (one crystal analyzed with multiple spots) display significant U-Th disequilibrium. Combining all disequilibrium U-Th zircon analyses yields an isochron age of 86 +37/–33 ka (MSWD = 1.3; n = 8; Fig. 6B). An alternative treatment of the data is to combine individual zircon spots with the whole-rock composition to calculate model crystallization ages (Fig. 6B). In this case, we obtained model crystallization ages between 19 +24/–22 ka and 121 +128/–80 ka, but whole-rock compositions for Cerro Prieto are likely affected by alteration (see following), and therefore this approach may result in age bias.

Xenocrystic zircon can be used to date the eruption age if ^{4}He has degassed completely during contact with the magma (Blondes et al., 2007). To test this approach, we analyzed individual xenocrysts extracted from the lava sample, as well as zircon separated from an ~10-cm-diameter baked mudstone enclave. This enclave

TABLE 2. WHOLE-ROCK COMPOSITIONS OF LAVAS AND INTRUSIVE ROCKS FROM CERRO PRIETO AND ROCA CONSAG

Sample:	M-203 1608	NL-1 1494	E-30 3027	E-30 3048	E-30 3069	M-194 2511	M-201 3080	M-201 3513	M-201 3534	M-203 3921	M-203 3954	M-203 3987	M-205 2957	CP05-2†	CP07-2§	RC01-24A§	RC01-24B§
Type:	Cerro Prieto well cuttings*													Cerro Prieto S dome	Cerro Prieto N dome	Roca Consag lava	
Latitude (°N):	32°23′ 33.463″	32°24′ 33.873″	32°23′ 57.086″	32°23′ 57.086″	32°23′ 57.086″	32°24′ 33.873″	32°24′ 34.768″	32°24′ 34.768″	32°24′ 34.768″	32°23′ 33.463″	32°23′ 33.463″	32°23′ 33.463″	32°25′ 41.608″	32° 25′25″	32° 24′60″	31° 06′45″	31° 06′45″
Longitude (°W):	115°11′ 12.434″	115°12′ 42.055″	115°12′ 51.315″	115°12′ 51.315″	115°12′ 51.315″	115°12′ 42.055″	115°10′ 23.248″	115°10′ 23.248″	115°10′ 23.248″	115°11′ 12.434″	115°11′ 12.434″	115°11′ 12.434″	115°9′ 4.567″	115° 18′5″	115° 18′30″	114° 29′17″	114° 29′17″
Major oxide (wt%)																	
SiO_2	56.0	56.0	71.9	57.0	54.5	57.7	58.2	58.6	51.1	62.2	61.8	61.3	58.4	68.6	67.2	67.0	67.8
TiO_2	1.51	1.45	0.36	1.45	1.70	1.96	1.65	1.85	2.54	0.87	0.79	0.75	1.82	0.49	0.52	0.37	0.38
Al_2O_3	16.8	16.7	14.0	15.3	16.1	15.4	16.6	15.0	15.3	18.1	18.0	15.6	16.6	15.1	14.7	16.9	17.0
Fe_2O_3 total	9.02	8.93	3.73	8.64	9.38	9.70	9.86	9.33	11.05	6.22	6.72	6.12	10.48	4.67	5.59	3.34	2.20
MnO	0.13	0.15	0.07	0.13	0.16	0.21	0.19	0.16	0.20	0.07	0.09	0.14	0.15	0.09	0.09	0.06	0.06
MgO	4.01	4.29	0.29	4.31	5.11	2.71	2.05	2.73	5.65	1.11	1.36	3.51	2.71	0.63	0.85	1.58	1.58
CaO	7.85	7.95	2.40	8.28	9.71	7.00	6.12	6.15	10.38	5.50	5.34	8.07	6.26	3.08	3.74	5.85	5.67
Na_2O	3.89	3.76	3.20	3.37	2.49	2.86	4.36	4.38	3.00	4.52	4.52	2.30	2.98	5.40	5.29	4.06	4.16
K_2O	0.80	0.82	4.05	1.50	0.82	2.40	0.98	1.77	0.76	1.37	1.34	2.23	0.63	1.60	1.49	0.65	0.68
P_2O_5	0.26	0.28	0.05	0.26	0.10	0.33	0.64	0.65	0.36	0.34	0.33	0.22	0.11	0.13	0.15	0.13	0.13
LOI (%)	–	–	–	–	–	–	–	–	–	–	–	–	–	1.90	–	0.15	0.03
Total	98.5	99.0	98.8	98.6	96.9	98.1	97.9	98.8	99.2	97.4	98.4	98.2	95.3	99.8	99.6	100.1	99.7
Trace elements (ppm)																	
Rb	11	14	53	32	20	64	15	52	29	27	26	38	11	26	23	10	10
Sr	228	226	326	206	182	255	347	173	162	456	370	280	226	280	317	783	540
Y	24	24	109	55	48	34	47	84	48	80	48	29	42	31	29	6.0	7.7
Zr	130	132	699	337	270	249	265	470	207	357	310	220	244	247	227	59	66
Nb	5.6	5.8	16	13	11	11	10	18	9.1	12	13	14	9.3	6.0	6.8	2.0	2.0
Ba	239	240	1019	242	166	638	434	281	62	461	524	670	358	734	720	300	295
La	12	13	69	21	18	21	20	29	11	32	25	33	17	25	27	7.9	8.4
Ce	27	27	146	50	38	47	46	70	30	68	52	66	40	57	53	15	16
Pr	3.2	3.3	18.0	6.4	5.3	5.7	5.9	9.4	4.4	8.4	6.4	7.4	5.3	–	6.5	2.0	2.0
Nd	15	16	79	29	23	26	27	46	22	38	31	31	23	–	25	7.8	8.0
Sm	3.8	3.7	17	8.1	6.4	4.5	7.0	12	6.4	9.8	7.4	5.8	6.0	–	5.6	1.5	1.8
Eu	0.86	0.93	2.7	1.0	1.3	0.68	1.5	2.1	1.7	1.8	1.5	1.0	1.5	–	1.6	0.5	0.6
Gd	3.7	3.9	18	7.8	7.4	5.7	7.0	13	7.1	11	7.2	5.3	6.6	–	5.4	1.2	1.6
Tb	0.66	0.55	3.1	1.6	1.4	1.1	1.4	2.5	1.4	2.3	1.4	0.91	1.2	–	0.90	0.20	0.25
Dy	4.6	4.5	21	11	8.3	6.2	9.0	15	9.2	16	8.9	5.7	8.2	–	5.6	1.0	1.4
Ho	0.87	0.83	4.2	2.1	1.9	1.4	1.8	3.1	1.9	3.1	1.8	1.3	1.6	–	1.2	0.20	0.29
Er	2.6	2.6	12	5.5	5.0	4.3	5.2	9.8	5.6	8.2	5.5	2.7	4.5	–	3.2	0.60	0.76
Tm	0.35	0.39	1.8	0.84	0.76	0.57	0.71	1.2	0.78	1.2	0.78	0.44	0.70	–	0.47	<0.1	0.11
Yb	2.7	2.7	14	5.5	5.6	4.1	5.5	10	5.2	7.6	5.0	3.3	5.1	–	2.9	0.40	0.69
Lu	0.36	0.38	2.1	1.0	1.1	0.55	0.80	1.4	0.72	1.2	0.87	0.27	0.77	–	0.46	0.05	0.11
$^{87}Sr/^{86}Sr$#	0.704441	0.704785	0.708698	–	–	–	–	–	0.704711	0.708185	0.708576	–	0.704815	–	0.7053749	0.703736	0.7036664
1 s.e.	0.000004	0.000005	0.000004	–	–	–	–	–	0.000006	0.000005	0.000005	–	0.000007	–	0.000005	0.000023	0.000005
$^{143}Nd/^{144}Nd$#	0.512867	0.5129213	0.5130754	–	–	–	–	–	0.5130937	0.5129439	0.5129346	–	0.512983	–	0.512671	0.512849	0.512811
1 s.e.	0.0000035	0.0000285	0.0000025	–	–	–	–	–	0.000002	0.0000035	0.000004	–	0.0000025	–	0.00001	0.0000085	0.000014
ε_{Nd}#	4.5	5.5	8.5	–	–	–	–	–	8.9	6	5.8	–	6.7	–	0.6	4.1	3.4
1 s.e.	0.3	0.6	0.2	–	–	–	–	–	0.2	0.3	0.3	–	0.2	–	0.2	0.2	0.3

*Major oxides by electron microprobe analysis; trace elements by secondary ion mass spectrometry using glass beads; analyses conducted at University of California–Los Angeles; last number in sample name indicates depth in m.

†Major oxides and trace elements by X-ray fluorescence (XRF); Pomona College.

§Major oxides by XRF; trace elements by inductively coupled plasma–mass spectrometry (ICP-MS); GeoAnalytical Laboratory Washington State University.

#Sr-Nd isotopes analyzed at Laboratorio Universitario de Geoquimica Isotopica (LUGIS), Instituto de Geofísica, Universidad Nacional Autónoma de México, except $^{87}Sr/^{86}Sr$ values for samples CP07-2 and RC01-24B (Scripps).

TABLE 3. U-Th ISOTOPIC COMPOSITIONS (ACTIVITIES IN PARENTHESES) FOR WHOLE ROCKS

Sample	Rock type	Location	^{238}U (ppm)		^{232}Th (ppm)		(^{230}Th)/(^{232}Th)		(^{238}U)/(^{232}Th)		(^{230}Th)/(^{238}U)		(^{234}U)/(^{238}U)	
CP05-2	Cerro Prieto lava	32°25′25″N, 115°18′05″W	0.597	0.0005	3.104	0.004	0.641	0.002	0.588	0.001	1.091	0.003	0.720	0.002
SB0402	Obsidian Butte lava	33°10′15″N, 115°38′03″W	5.99	0.0036	19.83	0.01	0.997	0.002	0.923	0.001	1.080	0.002	1.000	0.002
G2-112	Obsidian Butte lava (cuttings from geothermal well)	33°10′15″N, 115°38′08″W	5.67	0.0025	18.30	0.02	0.990	0.002	0.947	0.001	1.046	0.002	0.996	0.002
I70-24	Red Island granophyre xenolith	33°11′51″N, 115°36′44″W	3.482	0.0034	15.29	0.01	0.974	0.002	0.696	0.001	1.400	0.003	0.974	0.003

Note: Analytical errors are 1σ of the mean. Activity ratios were calculated by the decay constants used in Cheng et al. (2000).

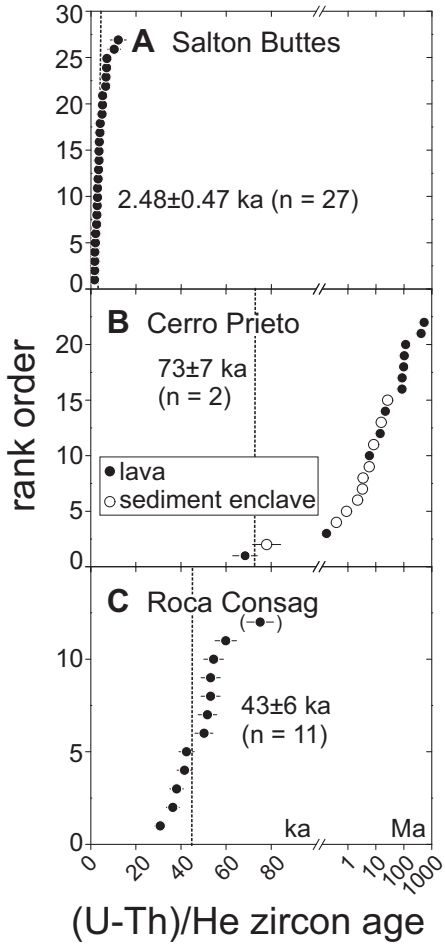

Figure 6. Individual (U-Th)/He ages and averages of (A) Salton Buttes (Schmitt et al., 2013); (B) Cerro Prieto, and (C) Roca Consag. Note that zircon crystals in B are xenocrystic (from a lava sample, and a sedimentary enclave), and that they have retained pre-eruptive ^{4}He. The youngest ages in B thus indicate a maximum eruption age.

was collected in the periphery of the Cerro Prieto dome where autobrecciated lava interfingers with surrounding playa sediments. In both cases, however, (U-Th)/He ages for xenocrystic zircons scatter widely between ca. 68 ka and ca. 550 Ma (Fig. 5B; Table 1). We attribute this to incomplete degassing of zircons, suggesting that the lava entrained the crystals (and enclaves) only shortly before cooling and solidification. The two youngest (i.e., most degassed) xenocrysts overlap within uncertainty and yield an average age of 73 ± 7 ka (n = 2). This is similar to the U-Th zircon crystallization age for the few non-xenocrystic zircons in Cerro Prieto lava (a maximum estimate for the eruption age). Collectively, these data strongly suggest that the eruption of Cerro Prieto occurred later than previously indicated based on comparatively imprecise K-Ar ages averaging ca. 100 ka (Reed et al., 1984), although the exact eruption age remains poorly constrained. Regardless, the presence of undegassed zircon xenocrysts has important implications for the timing of contamination of Cerro Prieto magmas en route to surface (see following).

Seven intermediate to microgranitic Cerro Prieto subsurface samples were processed, but only two microgranite samples in wells NL-1 and E-30 yielded zircon and allanite of late Pleistocene age (Table DR1 [see footnote 1]). The other samples contained exclusively older zircon, most likely from contamination of the cuttings by fragments from the overlying sediments (Table DR2 [see footnote 1]). For the microgranites, the resulting U-Th isochron ages overlap within uncertainty (36 +15/–14 ka and 42 +15/–14 ka (Fig. 6D). The MSWD value of 1.2 and 1.8 for NL-1 and E-30, respectively, suggests negligible nonanalytical scatter. Two-point model isochrons can be calculated using either Cerro Prieto lava or NL-1 allanite under the assumption that they were in isotopic equilibrium with zircon at the time of crystallization. In both scenarios, there would be a significant portion of zero-age zircon in the E-30 population, but because of low U concentrations, the precision of individual model ages is limited. In any case, the data for subsurface zircon are indicative of magma presence at shallow levels within the Cerro Prieto basin at ca. 40 ka or younger.

Roca Consag

Roca Consag zircons are overwhelmingly xenocrystic (Fig. 8B), with the youngest U-Pb zircon ages at ca. 120 ka (n = 2). One of these zircon crystals (RC z19) also displays U-series disequilibrium with (^{230}Th)/(^{238}U) = 0.85, attesting to its young age (Tables DR1 and DR2 [see footnote 1]). An outstanding feature in the Roca Consag zircon population is a dominant ca. 1 Ma age peak, significantly predating the younger population (Fig. 8B). This implies zircon recycling from a previously undiscovered Pleistocene source in the Wagner basin. The abundance of older crystals is likely due to a contribution of Colorado River sediment to the zircon population in Roca Consag lavas. The (U-Th)/He zircon ages for Roca Consag were calculated without disequilibrium corrections because their old crystallization ages imply secular equilibrium (Fig. 5C; Table 1). The average (U-Th)/He age is 43 ± 6 ka (n = 11; MSWD = 7.1 for individual 2σ errors of 16%). This average excludes the smallest grain (zRC-1), with its significant age uncertainty because of an

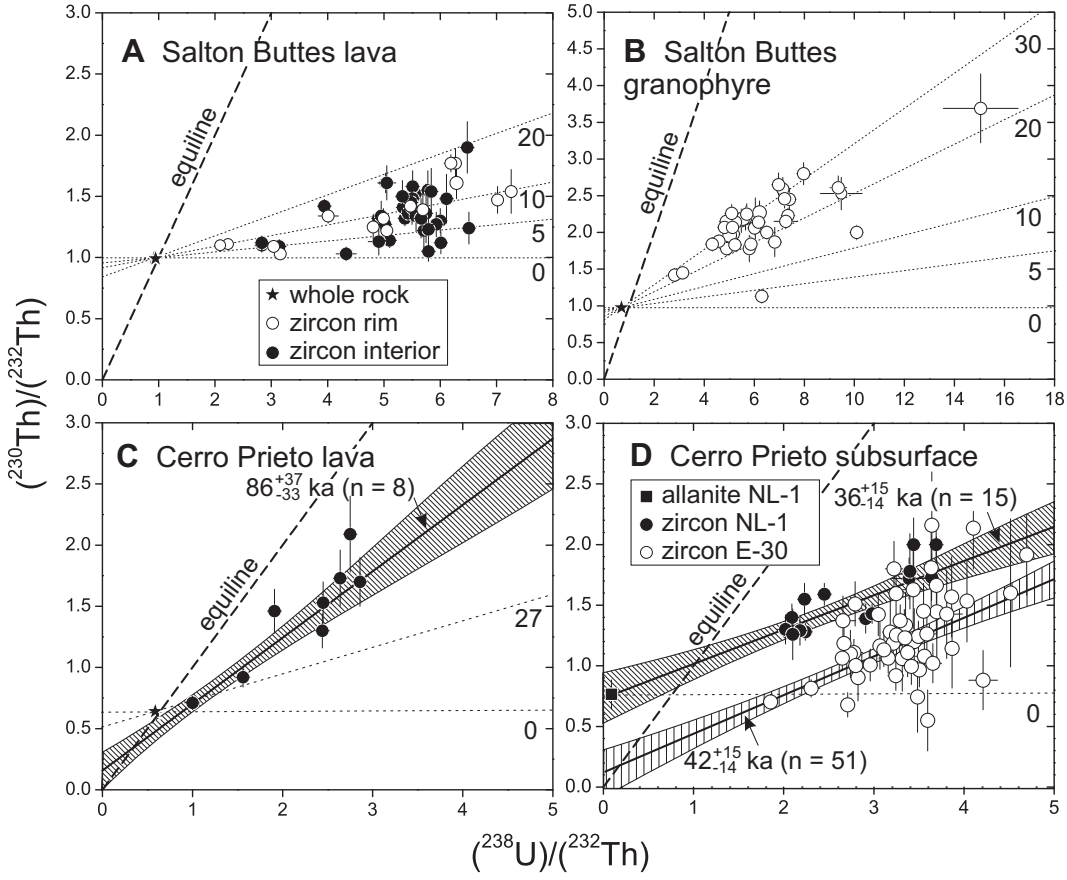

Figure 7. U-Th zircon and whole-rock data (activities indicated in parentheses) for (A) Salton Buttes lava, (B) Salton Buttes granophyre, (C) Cerro Prieto lava, and (D) Cerro Prieto subsurface intrusives. Data in A and B are from Schmitt et al. (2013); other data are from this study. Panels A and B show model isochron ages based on pairing zircon with whole-rock data. Panels C and D show zircon isochrons and error envelopes from regression of the zircon data (hatched), in comparison to paired whole-rock (allanite) and zircon model isochron ages.

unusually large α-ejection correction. We adopt this average of 43 ka as the eruption age of Roca Consag. The elevated MSWD is likely due to unrecognized systematic uncertainties regarding U and Th zonation of the crystals, and we account for this by multiplying the age uncertainty with the square-root of the MSWD.

CHEMICAL COMPOSITIONS

Whole-Rock Major and Trace Elements

New and published whole-rock analyses for northern Gulf of California igneous rocks indicate substantial compositional diversity ranging from basalt to high-silica rhyolite (Fig. 3; Table 2). A characteristic difference between Salton Buttes and Cerro Prieto is the strongly bimodal character of the Salton Buttes lavas and xenoliths, whereas Cerro Prieto surface and subsurface rocks have a dominantly intermediate population (Fig. 3). Despite these differences, end-member compositions are almost indistinguishable: The least altered (based on low-K) gabbros from Cerro Prieto are equivalent to those at the Salton Buttes, and high-silica end-member compositions (Cerro Prieto microgranite; Salton Buttes rhyolite and granophyre) equally overlap.

A kinked trend in Al_2O_3 versus SiO_2 with a peak at SiO_2 = 62 wt% exists for Cerro Prieto intermediate rocks, which also shows a subtle break in slope for CaO and MgO versus SiO_2. This clearly rules out binary mixing as a mechanism for generating intermediate compositions. The trends in Figure 3 are broadly consistent with the increasing abundance of plagioclase in the fractionating assemblage, but similar variations can result from variable degrees of partial melting of hydrous basalt at low to intermediate H_2O partial pressure $P(H_2O)$ (<170 MPa; Thy et al., 1990). Importantly, experimental glass compositions for partial melting of hydrated basalt under higher $P(H_2O)$ between 300 and 500 MPa (Thy et al., 1990) are higher in Al_2O_3 than observed for Cerro Prieto rocks (Fig. 3B). K_2O broadly increases with increasing SiO_2, but most compositions plot above values permissive for closed-system fractional crystallization of MORB. Although major-element compositional trends are broadly similar for MORB fractional crystallization and partial melting of MORB-type lower crust (France et al., 2010), the presence of excess K_2O (Fig. 3E) suggests that closed-system fractional crystallization of a MORB parent cannot be the sole process that produced felsic melts in the northern Gulf of California. For the basaltic xenoliths, the presence of amphibole indicates higher degrees of hydration, compared to clinopyroxene-bearing gabbros in Cerro Prieto wells.

Among trace elements plotted in Figure 3, Sr shows significant scatter and deviates from the Ca trend. We attribute Sr mobility to hydrothermal alteration, which limits the use of Sr as a petrogenetic indicator (this also holds for $^{87}Sr/^{86}Sr$; see following). Zr abundances generally increase with SiO_2, suggesting zircon-undersaturated conditions throughout most of the magmatic differentiation path. For Cerro Prieto, this is consistent with the scarcity or absence of zircon in intermediate rocks and their exclusive presence in microgranites.

MORB-normalized trace elements for mostly mafic to intermediate compositions (Cerro Prieto and Roca Consag; Fig. 3) are enriched in fluid-compatible elements—typically interpreted as an indicator for fluid addition to the mantle during subduction. Comparison with regional subduction-related volcanic rocks (San Luis Gonzaga volcanic field; Martín et al., 2000) shows that similar enrichments exist for equivalent SiO_2 (ranging between ~54 and ~67 wt%), including a prominent negative Nb anomaly. Positive Sr anomalies indicate the presence of cumulate plagioclase in some intrusive samples.

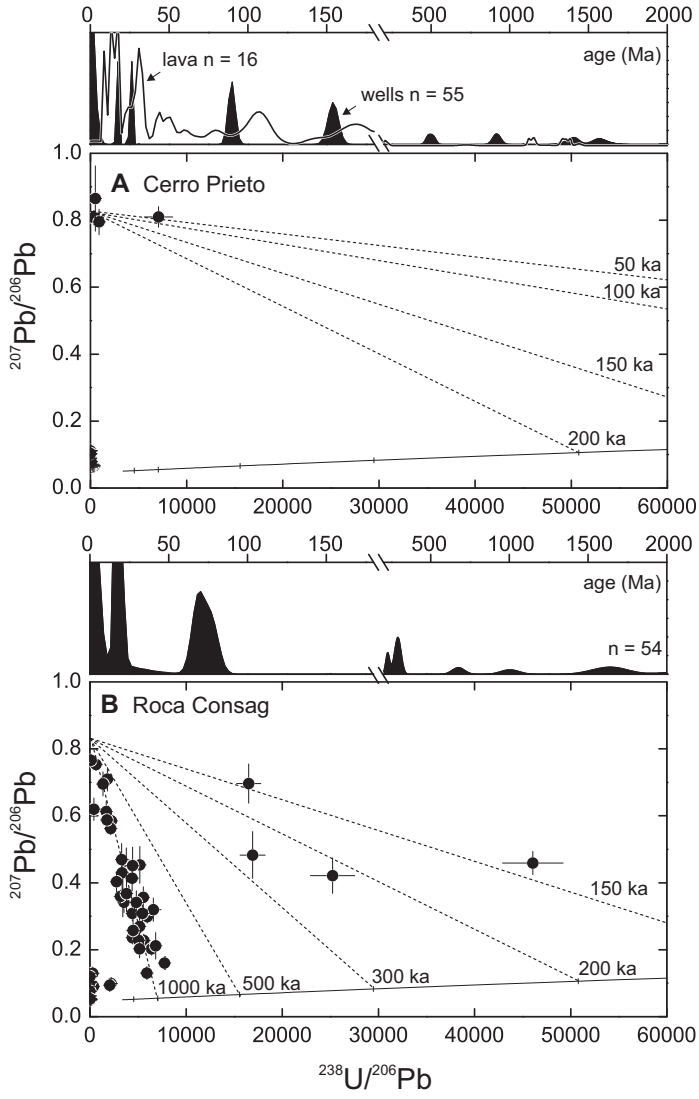

Figure 8. U-Pb zircon ages for (A) Cerro Prieto and (B) Roca Consag. Large panels are $^{207}Pb/^{206}Pb$ vs. $^{238}U/^{206}Pb$ concordia diagrams showing data uncorrected for common Pb and isochrons for mixtures between anthropogenic common Pb ($^{207}Pb/^{206}Pb$ = 0.8283) and radiogenic Pb (ages in ka). Smaller panels are relative probability plots for zircon ages (ages in Ma) showing zircons from (A) Cerro Prieto lava and well samples and (B) Roca Consag lava. Zircon in Cerro Prieto igneous well samples is likely derived from wall rock and is interpreted to represent the detrital age distribution of Colorado River and local sediment sources. The dominant ca. 1 Ma peak in Roca Consag results from crystal recycling from an unidentified source that is buried and submerged in the northern Gulf of California.

Whole-Rock Isotopic Compositions

Relative to bulk earth, ε_{Nd} is elevated for all magmatic compositions with the most positive values in basaltic xenoliths from Salton Buttes and microgabbros from Cerro Prieto (ε_{Nd} = +8.9; Fig. 9; Table 2). These values closely overlap with those of regional MORB lavas (East Pacific Rise, and Alarcon basin), and they imply that the mantle source underneath the Salton Trough and Cerro Prieto basin is asthenospheric mantle, similar to the mantle underneath oceanic spreading systems (cf. Lizarralde et al., 2007). Cerro Prieto and Roca Consag lava samples fall on a trend with anticorrelated $^{87}Sr/^{86}Sr$ and ε_{Nd}, as expected for magmatic mixing and/or assimilation involving crustal sources such as Peninsular Ranges batholith or metasedimentary rocks (Fig. 9). Subsurface samples (including Cerro Prieto microgabbros) are displaced from the depleted-mantle trend toward elevated $^{87}Sr/^{86}Sr$ (Fig. 9). This is also the case for the Salton Buttes rhyolite lava and a granophyre xenolith (Fig. 9). We interpret this as the result of Sr exchange with sedimentary wall rock during hydrothermal alteration in an active geothermal field. Although no consistent trend in ε_{Nd} versus SiO_2 exists over the entire data set (Fig. 3H), there are two delineating end members: (1) ε_{Nd} is nearly invariant over the entire range of SiO_2 for Cerro Prieto gabbro and microgranite, which is indicative of closed-system magma differentiation; and (2) ε_{Nd} systematically decreases with increasing SiO_2 for intermediate Cerro Prieto samples, which potentially indicates that fractional crystallization is coupled to assimilation-fractional crystallization (AFC).

U-Th whole-rock isotopic compositions for Salton Buttes and Cerro Prieto plot to the left of the equiline (Fig. 6; Table 3). This is characteristic for magmas generated by decompression melting of the mantle, in the absence of a high-U fluid-mobile component. Their $(^{238}U)/(^{232}Th)$ overlaps with MORB compositions from the East Pacific Rise at 21°N, with the exception of the extremely low U/Th for Cerro Prieto lava. This is likely due to secondary alteration (causing U-loss), which is also indicated by strong $(^{234}U)/(^{238}U)$ disequilibrium, and thus Cerro Prieto lava is not further considered here. The comparatively low $(^{230}Th)/(^{238}U)$ relative to MORB could indicate protracted differentiation time scales (i.e., aging of the source over 200 k.y.). We, however, favor mixing with and/or assimilation of crustal rocks in secular equilibrium because of the isotopic heterogeneity in ε_{Nd} ($^{143}Nd/^{144}Nd$) and $^{87}Sr/^{86}Sr$ (Fig. 10) and the decrease in ε_{Nd} with increasing SiO_2 (Fig. 3H).

Zircon Trace Elements and Oxygen Isotopes

Because hydrothermal overprint affected subsurface samples, we used trace elements and oxygen isotopic compositions of zircon as petrogenetic indicators (Figs. 11–13; Tables DR3 and DR4 [see footnote 1]). Zircon's imperviousness to hydrothermal alteration is demonstrated by the preservation of highly variable oxygen isotopic compositions in detrital zircon crystals from the same depth intervals as the magmatic zircons from dikes and sills encountered in the Cerro Prieto and Salton Sea wells. The heterogeneity in $\delta^{18}O$ for detrital zircon contrasts with the oxygen isotopic homogeneity of young

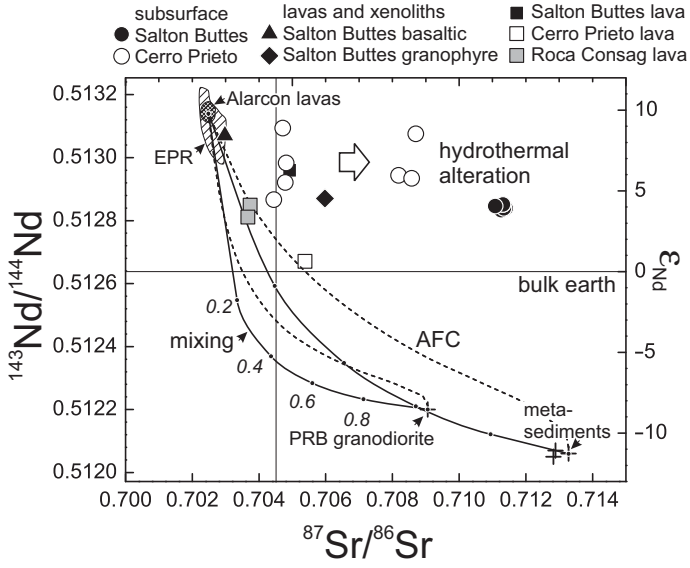

Figure 9. Nd vs. Sr isotopic compositions of northern Gulf of California igneous rocks in comparison with East Pacific Rise (EPR) and Alarcon lavas (Castillo et al., 2002, and references therein). Model curves for mixing and assimilation-fractional crystallization (AFC) are indicated for Peninsular Ranges Batholith (PRB) or metasedimentary rocks (Herzig and Jacobs, 1994). Samples plotting to the right of these curves are presumably affected by hydrothermal alteration caused by $^{87}Sr/^{86}Sr$ exchange with country-rocks due to high fluid mobility of Sr, whereas $^{143}Nd/^{144}Nd$ (ε_{Nd}) remains largely constant. Data sources: this study, Herzig and Jacobs (1994), and Schmitt and Hulen (2008).

magmatic zircons in individual samples, indicating the absence of oxygen isotopic exchange between zircon and fluids in the modern geothermal system (Fig. 12). Magmatic zircon $\delta^{18}O$ values for Salton Buttes lavas and basaltic xenoliths (Schmitt and Vazquez, 2006) fall into a broad range averaging ~5‰ (±1‰; Fig. 12). This is broadly comparable to two zircons in Cerro Prieto lavas that were sufficiently large to be analyzed for $\delta^{18}O$ (Fig. 12). Salton Sea subsurface lavas (Schmitt and Hulen, 2008) are also similar in their zircon $\delta^{18}O$ values (Fig. 12), and overall, these values overlap with those of oceanic crustal zircon (Grimes et al., 2011). Cerro Prieto microgranite zircons are strongly depleted in $\delta^{18}O$, with average values of ~2‰. These values fall below mantle values (5.3‰ ± 0.3‰; Valley, 2003) and require substantial exchange with meteoric water in the source rocks for the microgranite lavas, consistent with similarly low values for Salton Buttes granophyre zircons (Schmitt and Vazquez, 2006). Roca Consag Quaternary zircon averages $\delta^{18}O$ = 6.0‰ (±0.9‰; Fig. 12), the highest values for non-xenocrystic zircon present in the northern Gulf of California samples, indicating a comparatively high proportion of continental crust in the source magma for the ca. 1 Ma Roca Consag zircon population.

Zircon trace elements (including Ti and REEs; Table DR3 [see footnote 1]) for Salton Buttes (Schmitt and Vazquez, 2006) and Cerro Prieto overlap with values for oceanic crustal zircon (Fig. 11). In the case of zircon from rhyolite and dacite lavas, trace-element compositions straddle the lower limit determined for continental crustal zircon, whereas zircons from Salton Buttes basaltic xenoliths and Cerro Prieto microgranites plot below the continental crustal field. Roca Consag zircon crystals in the ca. 1 Ma age population, by contrast, have trace-element compositions that are consistent with continental crustal sources. This is also the case for detrital zircon crystals from Cerro Prieto wells. Zircon crystallization temperatures of 700–800 °C were estimated from Ti-in-zircon thermometry (Fig. 13; Ferry and Watson, 2007). These are temperature minima because they were calculated for titanium oxide activity a_{TiO_2} = 1 and silica activity a_{SiO_2} = 1. The presence of quartz in the microgranites indicates a_{SiO_2} = 1, but a_{TiO_2} is subunity because of the absence of rutile. If, for example, zircon crystallization would occur at a_{TiO_2} = 0.5 and a_{SiO_2} = 1, this would elevate zircon crystallization temperatures by ~70 °C (Ferry and Watson, 2007). One exception is zircon in quartz-free basaltic xenoliths; in this case, subunity a_{SiO_2} would be compensatory with a_{TiO_2} <1. Regardless of these uncertainties, zircon Ti abundances and model crystallization temperatures are similar to those of oceanic zircons (Fig. 13). This is an important constraint on the conditions of zircon crystallization in basalt-derived melts that requires temperatures significantly below basalt liquidus temperatures.

DISCUSSION

Timing of Synrift Magmatism in the Northern Gulf of California

New and recently published (U-Th)/He, U-Th, and U-Pb ages constrain late Pleistocene to Holocene pulses of magmatism within the northern Gulf of California rift basins: Surface

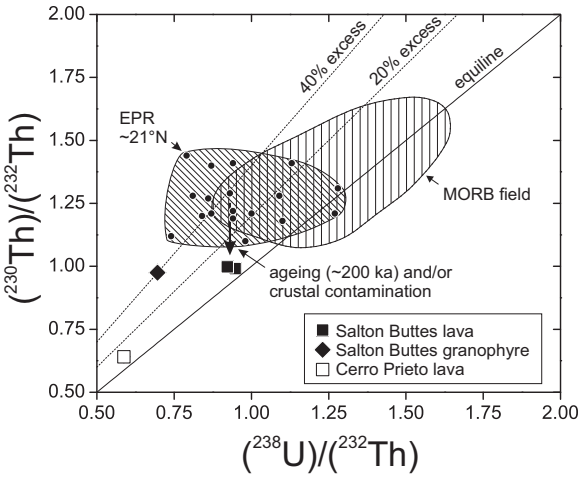

Figure 10. U-Th whole-rock activity ratios (indicated by parentheses) in comparison with East Pacific Rise and mid-ocean-ridge basalt (MORB) compositions. A schematic aging trend for MORB with 40% excess ^{230}Th is indicated, but a similar trend can result from contamination with secular equilibrium rocks. Note that Table 3 lists Cerro Prieto lava with low $(^{234}U)/(^{238}U)$ suggestive of alteration.

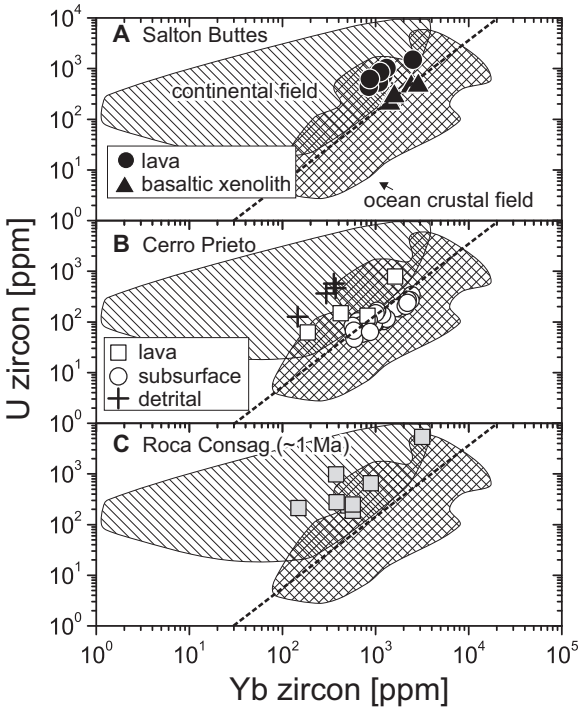

Figure 11. Zircon U vs. Yb abundances for northern Gulf of California igneous rocks. Fields for continental and oceanic zircon are from Grimes et al. (2007).

volcanism in the Salton Buttes occurred only ~2.5 k.y. ago (Schmitt et al., 2013), the eruption of Cerro Prieto is <80 ka as indicated by the least radiogenic ^{4}He in xenocrystic zircon, and Roca Consag erupted at ca. 40 ka (this study). These ages for volcanism in these rift basins imply a very recent heat pulse for the associated geothermal reservoirs. This has been previously proposed on the basis of detrital K-feldspar thermochronology for the Salton Sea geothermal reservoir, indicating present-day peak temperatures that could not have been maintained for more than a few thousand years (Heizler and Harrison, 1991). Moreover, young U-Th zircon crystallization ages from subsurface samples indicate that intrusive magmatism was coeval with eruptive activity, both within the Salton Trough and Cerro Prieto basins. The combined evidence from U-Th zircon crystallization ages reveals protracted magmatic activity within these rift basins throughout the late Pleistocene into the Holocene.

With the exception of Roca Consag (see following), all rocks studied here have a significant abundance of juvenile zircons. In samples where late Pleistocene to Holocene zircons are present, they lack xenocrystic cores. Although abundant older crystals exist in subsurface samples and lavas such as Cerro Prieto, there are two indications that these are not truly magmatic xenocrysts: (1) In the case of cuttings from subsurface igneous rocks, the abundance of older crystals correlates with the (visually estimated) abundance of sediment fragments that were entrained by air-drilling, and (2) in lava samples, there is residual radiogenic ^{4}He in pre-Quaternary zircons, which indicates that these crystals were only briefly in contact with the melt, and were likely entrained during the eruption.

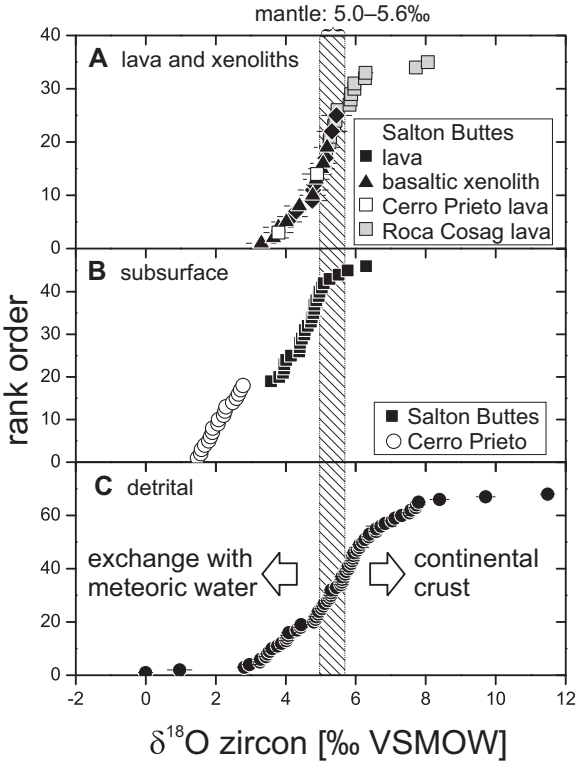

Figure 12. Zircon δ^{18}O compositions for northern Gulf of California igneous rocks (this study; Schmitt and Vazquez, 2006; Schmitt and Hulen, 2008). Mantle-derived zircons (via closed-system fractionation of mantle melts) fall in a narrow compositional range around 5.3‰ (Valley, 2003); deviations to lower values require exchange with meteoric water, whereas higher values are indicative of continental crustal origins. VSMOW—Vienna standard mean ocean water.

In previous studies, older pulses (ca. 400–500 ka) of volcanic and intrusive magmatism have been documented in the Salton Trough subsurface in close proximity to the Salton Buttes (Schmitt and Hulen, 2008). These older pulses, however, did not contribute to the zircon population in the younger lavas and xenoliths. This implies that silicic intrusions are small in volume and segregated. Alternatively, preexisting zircon could have been resorbed by heating and addition of mafic magmas in subsequent intrusive episodes. An intriguing observation in this context is the abundance of ca. 1 Ma zircon crystals with a continental crustal signature in Roca Consag lavas. Roca Consag xenocrystic zircon crystals lack significant radiogenic ^{4}He despite their age. Thus, they must have degassed, potentially during magmatic assimilation. The source of the dominant ca. 1 Ma component in Roca Consag lavas remains enigmatic in the absence of any rocks of equivalent age onshore. Quartz-phyric volcanic rocks with a K-Ar feldspar age of 1.4 ± 0.5 Ma have been encountered in the Altar basin (northwestern Sonora) in an exploratory well at ~3.8 km depth (Pacheco et al., 2006). At present, we can only speculate that the ca. 1 Ma Roca Consag zircons originated from felsic magmas, which, based on high δ^{18}O and trace-element patterns for zircon, had a more continental affinity than younger zircon-crystallizing magmas in the Salton and Cerro Prieto basins. This permits us

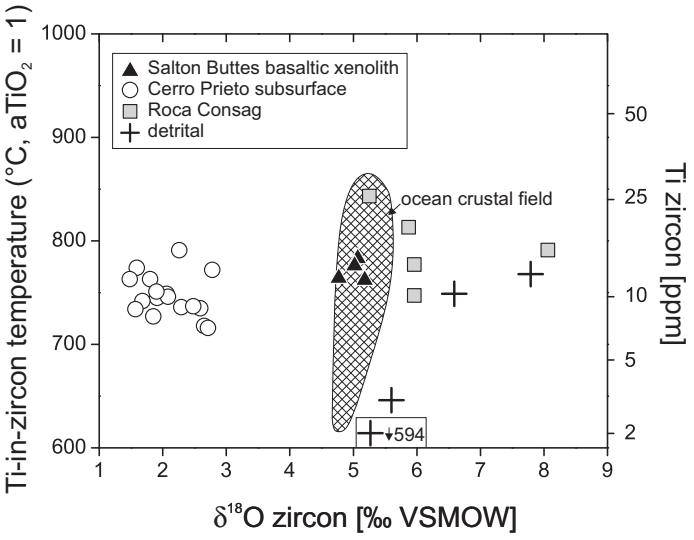

Figure 13. Zircon $\delta^{18}O$ vs. Ti-in-zircon temperatures for northern Gulf of California igneous rocks. Oceanic field is from Grimes et al. (2011). VSMOW—Vienna standard mean ocean water.

to bracket the onset of magmatism with oceanic affinity in the northern Gulf of California between ca. 1 Ma ("continental crustal" zircons in Roca Consag) and ca. 0.5 Ma ("oceanic" zircons in buried Salton Buttes lavas), although we acknowledge that this is highly tentative because of the very limited availability of igneous rocks for this critical age range.

MORB versus Continental Crustal Sources

Geophysical models remain ambiguous with regard to the state of continental rupture and oceanic spreading in the northern Gulf of California: Extrapolation of modern plate velocities implies largely uniform amounts of extension along the entire rift zone, but direct evidence for Pliocene–Pleistocene oceanic crust formation such as magnetic striping is lacking (Lonsdale, 1989). Early proponents of oceanic crustal formation in the northern Gulf of California have reasoned, on the basis of compositional and isotopic similarities between MORB and basaltic xenoliths in the Salton Buttes, that rifting has proceeded there to a stage of oceanic crust formation (Herzig and Jacobs, 1994; Robinson et al., 1976). The origins of intermediate to silicic magmas and their relationships to basaltic magmas, however, have remained ambiguous. Crustal melting has been previously proposed (e.g., Reed et al., 1984), but this was based on geochemical indicators that subsequently proved to be unreliable, especially for rocks for which the composition may have been altered by hydrothermal activity or contaminated during emplacement in unconsolidated sediments: $^{87}Sr/^{86}Sr$ in particular is vulnerable to contamination because Sr typically decreases with differentiation, and thus differentiated rocks are more easily affected by entrainment of crustal xenoliths or secondary alteration. Consequently, we interpret the strong displacement of subsurface rocks to the right of plausible magmatic mixing/assimilation trends in the $^{87}Sr/^{86}Sr$ versus ε_{Nd} diagram (Fig. 9; Schmitt and Hulen, 2008) as a result of Sr-isotopic exchange between rock and hydrothermal fluid. Hence, for constraining magma sources, we restrict our discussion in the following to fluid-insensitive indicators such as whole-rock Nd isotopes, and trace elements and oxygen isotopes in magmatic zircons.

Salton Buttes and Cerro Prieto have ε_{Nd} values in the least differentiated (basaltic) rocks that are strikingly similar to East Pacific Rise and Alarcon lavas, where seafloor spreading is unambiguous (Fig. 9). This suggests that basaltic magmas along strike of the Gulf of California share a common asthenospheric mantle source. Even some of the most felsic rocks have Nd-isotopic compositions that are identical to those of basalts (Fig. 9). Although some of the intermediate and felsic rocks are displaced to lower ε_{Nd} values relative to regional mantle-derived rocks, they lack a clear signature for anatexis of continental crust as a significant contributor to rift-related magmatism in the northern Gulf of California (Fig. 9). Because xenocrystic zircons in these lavas frequently retain pre-eruptive ^{4}He, caution has to be exercised in interpreting shifts to lower ε_{Nd} as true magmatic mixing or assimilation trends. Instead, this trend could result from shallow contamination of the lavas during emplacement onto unconsolidated sediment. Regardless of the ambiguity whether mixing and/or assimilation took place via continental crustal anatexis or entrainment of soft sediments, binary mixing calculations indicate that even the most contaminated lavas contain at most ~20% of a continental crustal end member (Fig. 9).

In addition to fractional crystallization of MORB-type magmas with minor assimilation of continental crustal rocks, oxygen isotopes in zircon require another, previously largely overlooked, process in the genesis of rift-related magmas in the northern Gulf of California. The strong depletion of $\delta^{18}O$ in microgranitic zircons coupled with high ε_{Nd} indicate remelting of a hydrothermal MORB-type crust. Thus, juvenile crust of oceanic affinity must have exchanged with meteoric waters during episodes of hydrothermal alteration, resulting in $\delta^{18}O$ depletion relative to mantle values. Remelting of this hydrothermally altered oceanic crust through reinjection of fresh mafic magma is a viable scenario to generate rhyolitic melts that directly inherit the low $\delta^{18}O$ and MORB-like ε_{Nd} of their source. Such low $\delta^{18}O$ rhyolites are common in oceanic rifts such as Iceland (e.g., Martin and Sigmarsson, 2007), and some oceanic plagiogranites also display depleted $\delta^{18}O$ values (Grimes et al., 2011).

The combination of high ε_{Nd} and low $\delta^{18}O$ clearly rules out anatexis of any plausible continental crustal sources for Salton Sea and Cerro Prieto felsic magmas (Figs. 10 and 12). This is further supported by zircon trace elements: Low U relative to Yb distinguishes most Cerro Prieto microgranite zircons and those from Salton Buttes basaltic xenoliths from typical continental crustal zircon (Fig. 11). We emphasize that the zircon evidence ($\delta^{18}O$ and trace elements) is crucial for detecting this mechanism because zircon records a primary magmatic signal that is not overprinted by alteration in the modern hydrothermal system. By contrast, whole-rock enrichment patterns in fluid-mobile trace elements are less reliable, and could be erroneously interpreted as inherited from a hydrated mantle source, similar to that of subduction zones (Fig. 4). Based on whole-rock data alone, it thus would be difficult to distinguish between source enrichment (i.e., due to fluid addition from a subducted slab) and hydrothermal alteration of basaltic crustal precursor rocks as the cause of the enrichment of fluid-mobile trace elements (Fig. 4). By contrast, zircon geochemistry is indicative of a MORB-like source, which is characterized by lower U/Yb compared to arc-like and continental crustal rocks (Fig. 11).

Felsic Magmas in Incipient Oceanic Spreading Centers with Thick Sedimentary Cover

Having established a dominantly MORB-type source for mafic magmas in the northern Gulf of California from Nd-isotopic evidence, we now discuss the styles of differentiation in the context of other occurrences of differentiated magmas in mid-ocean-ridge environments. There, basaltic magmas are known to undergo significant differentiation, which is recorded by evolved intrusive rocks in oceanic crustal segments (plagiogranites). Only occasionally and in specific tectonic settings, such as propagating rift tips or rift-transform intersections, have felsic mid-ocean-ridge lavas been documented (e.g., Schmitt et al., 2011; Wanless et al., 2010). In the Gulf of California province, oceanic spreading occurs in short (tens of kilometers) segments separated by transform faults, which is a broadly similar setting to rift-transform intersections where felsic mid-ocean-ridge lavas have erupted (e.g., Juan de Fuca; Schmitt et al., 2011). Fractional crystallization of parental basalt is a potential mechanism to generate SiO_2-rich magmas, but this is inconsistent with geochemical data such as the observed K_2O enrichments, and oxygen isotopic depletion, which cannot be explained by closed-system differentiation of pristine MORB. The presence of rhyolite melt pockets in basaltic xenoliths from the Salton Buttes is direct petrographic evidence that remelting of hydrated (amphibole-bearing) mafic rocks is viable for producing felsic melts (Robinson et al., 1976). Felsic melt pockets are also highly amenable to zircon crystallization (Schmitt and Vazquez, 2006). A comparison with glass compositions experimentally produced for partial melting of basalt in the presence of H_2O indicates that remelting occurred under fairly low H_2O (and total) pressures, likely <170 MPa (Fig. 3B; Thy et al., 1990). This places the region of basaltic intrusion and remelting at a depth shallower than ~7 km, close to the base of low-density and low-seismic-velocity basin fill (Fig. 14; Fuis et al., 1984; Parsons and McCarthy, 1996).

Given the limited range in $\delta^{18}O$ of pristine MORB magmas, fractional crystallization is expected to produce intermediate to rhyolitic magmas that are only moderately elevated (by ~1‰–2‰) in $\delta^{18}O$ relative to the parental magma compositions, translating into a narrow range of mantle-derived zircon (Valley, 2003) when accounting for oxygen isotopic fractionation between zircon and melt (~1‰ at 800 °C; Trail et al., 2009). Magmatic compositions of Cerro Prieto and Salton Buttes lavas marginally overlap with this range, but their $\delta^{18}O$ values are on average lower than mantle. Unequivocally low-$\delta^{18}O$ zircons, such as crystals in Cerro Prieto microgranites and Salton Buttes granophyres, however, require a low-$\delta^{18}O$ source compared to mantle-derived magmas. Isotopically light oxygen typical for near-surface waters must have infiltrated a mafic source (inferred from high ε_{Nd}) prior to remelting and differentiation.

Thus far, we have identified two key similarities for magmas in the Salton Trough and Cerro Prieto (Roca Consag lavas appear to be distinct, but because of limited exposure and sampling, this is a tentative conclusion): Mafic end members are similar and MORB-like, and melting of a MORB-type crust has occurred subsequent to hydrothermal alteration, producing high-silica rhyolite magmas. As noted previously, a conspicuous distinction between both magmatic systems is that magma compositions are strongly bimodal in the Salton Trough, whereas intermediate intrusive and extrusive rocks exist at Cerro Prieto. Cerro Prieto intermediate rocks (barring E-30 3027 m microgranite) show a trend to lower ε_{Nd} with increasing SiO_2 (Fig. 3H), which can be explained by AFC involving minor amounts of continental crustal rocks. Binary mixing between high-silica rhyolites and basalts can be ruled out because the intermediate compositions deviate from isotopic and trace-element mixing trajectories (Fig. 3). The ε_{Nd} values for intermediate rocks from Cerro Prieto and Salton Sea overlap, suggesting that the overall amount of assimilation is similar in both systems, although Cerro Prieto lavas have lower ε_{Nd}. The presence of only partially ^4He-degassed detrital zircon crystals in Cerro Prieto lavas, however, indicates that at least some continental crustal material was incorporated late, and not via anatectic assimilation at depth (Fig. 5). This urges caution in using whole-rock analyses, which may have become contaminated upon ascent and emplacement at shallow depth, in particular during magma interaction with unconsolidated sediment.

There is strong evidence based on oxygen and Nd isotopes for remelting of young MORB-type crust as a source for felsic magmas, as indicated by the horizontal trend in ε_{Nd} versus

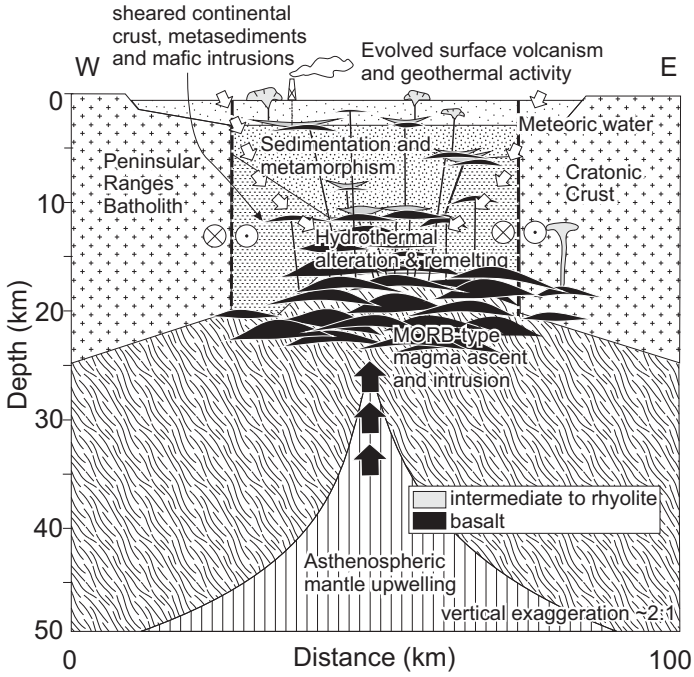

Figure 14. Schematic cross section illustrating the magmatic processes in northern Gulf of California rift basins. Active magmatism involves mid-ocean-ridge basalt (MORB)–type parental magmas derived from partial melting of decompressing asthenosphere, with intermediate and rhyolitic magmas generated by fractional crystallization and remelting of hydrothermally altered mafic intrusions. Only late Pleistocene (ca. 1 Ma) zircons from Roca Consag indicate minor melting and/or assimilation of continental crust. Underlying model of crustal structure from gravity variations is modified from Parsons and McCarthy (1996).

SiO_2 (Fig. 3). Conclusive evidence for continental crustal anatexis as a significant source for magmatism in the northern Gulf of California is absent, despite minor degrees of crustal assimilation in some of the felsic lavas. This conclusion holds for post–1 Ma magmas, whereas ca. 1 Ma xenocrystic zircons in Roca Consag lavas display some continental affinity. Even where minor assimilation is indicated by lower ε_{Nd} values, this would at most amount to an ~20% crustal contribution (Fig. 9). Major elemental compositional differences between Salton Sea and Cerro Prieto exist, but they are of secondary relevance with regard to the main mechanisms of magma production in the mantle, and remelting of hydrothermally altered mafic crust.

The deeper parts of the basin crust in the northern Gulf of California are postulated to be dominated by basaltic intrusions, yet unlike basins in the southern Gulf of California, surficial basalts are absent. Thick sedimentary blanketing thus plays an important role for magmatic differentiation in rifts (Fig. 14), but not for basaltic magma generation, which is compositionally homogeneous along the entire extent of the Gulf of California rift zone (cf. Lizarralde et al., 2007). A major effect of the sedimentary basin infill is that it controls the neutral buoyancy level of magmas. Felsic magmas have lower density and tend to ascend to shallower levels, whereas basaltic melts reach neutral buoyancy at deeper levels within the thick sedimentary pile. This is consistent with the presence of intermediate to felsic compositions of samples collected both in subaerial and submarine volcanoes in the northern Gulf of California. By contrast, basaltic to andesitic eruptions have only been reported in the Ballenas Channel and the lower Delfin basin, where sedimentary deposits are thin (Martín et al., 2013). As a second effect of high sedimentation rates, we propose that thermal insulation by sediments facilitates subsequent remelting of basaltic intrusions, which is aided by hydration during low-temperature water-rock interactions, also lowering the $\delta^{18}O$ of the rocks.

CONCLUSIONS

Late Pleistocene to Holocene magmatism in the northern Gulf of California rift zone occurs in an environment characterized by high deposition rates of continent-derived detritus in narrow rift basins. Intrusion of this sedimentary package by mafic to silicic magmas causes thermal overprint and metamorphism, but falls short of generating voluminous anatexis of sediments. Hydration of juvenile mafic crust via deep circulation of meteoric fluids occurs in these basins, lowering the oxygen isotopic composition and the solidus of mafic rocks, which readily exchange oxygen with fluids. Remelting of newly formed oceanic-type crust underlying the sediments by intrusion of mantle-derived basalts is the dominant origin of felsic magmas in this rift. Continental crustal sources, or subduction-metasomatized mantle, thus contribute only marginally, if any, to melt generation. In this respect, the lower crust in the rift basins of the northern Gulf of California—albeit distinct from typical oceanic crustal sequences by a thick overburden of sediments—has become fundamentally oceanic in nature. This study emphasizes the importance of single-crystal zircon analysis to see through the effects of near-surface contamination by soft sediment–magma interaction, and pervasive hydrothermal alteration, which are typical for rift basins filled by continent-derived detritus.

ACKNOWLEDGMENTS

We thank Julio Alvarez Rosales and staff at Comisión Federal de Electricidad for their support in obtaining well cuttings from Cerro Prieto. Michael Huh is thanked for assistance with petrographic logging of well cuttings and fused bead preparation. We thank Gabriel Rendón for zircon mineral separation and Pat Castillo for whole-rock Sr-isotope analysis of Cerro Prieto and Roca Consag lavas. We also thank Peter Schaaf and Gabriela Solís Pichardo, both at LUGIS, UNAM, for assistance with running the Finnigan MAT262. We are also thankful for comments by reviewers Andy Barth, Teresa Orozco-Esquivel, and Associate Editor Brian McConnell, as well as Science Editor Nancy Riggs. This work was supported by grants through UC-MEXUS CN 07-60 and National Science Foundation MARGINS (grant EAR-0948162). The ion microprobe facility at the University of California–Los Angeles is partly supported by a grant from the Instrumentation and Facilities Program, Division of Earth Sciences, National Science Foundation. U-Th isotopic determinations were supported by Taiwan ROC National Science Council grants (NSC 100-2116-M-002-009, 101-2116-M-002-009, and NTU 102R7625 to Chuan-Chou Shen).

REFERENCES CITED

Aguillon-Robles, A., Calmus, T., Benoit, M., Bellon, H., Maury, R.O., Cotten, J., Bourgois, J., and Michaud, F., 2001, Late Miocene adakites and Nb-enriched basalts from Vizcaino Peninsula, Mexico: Indicators of East Pacific Rise subduction below southern Baja California?: Geology, v. 29, p. 531–534, doi:10.1130/0091-7613(2001)029<0531:LMAANE>2.0.CO;2.

Anovitz, L.M., Elam, J.M., Riciputi, L.R., and Cole, D.R., 1999, The failure of obsidian hydration dating: Sources, implications, and new directions: Journal of Archaeological Science, v. 26, p. 735–752, doi:10.1006/jasc.1998.0342.

Batiza, R., 1978, Geology, petrology, and geochemistry of Isla Tortuga, a recently formed tholeiitic island in Gulf of California: Geological Society of America Bulletin, v. 89, p. 1309–1324, doi:10.1130/0016-7606(1978)89<1309:GPAGOI>2.0.CO;2.

Bellon, H., Aguillon-Robles, A., Calmus, T., Maury, R.C., Bourgois, J., and Cotten, J., 2006, La Purisirna volcanic field, Baja California Sur (Mexico): Miocene to Quaternary volcanism related to subduction and opening of an asthenospheric window: Journal of Volcanology and Geothermal Research, v. 152, no. 3–4, p. 253–272, doi:10.1016/j.jvolgeores.2005.10.005.

Benoit, M., Aguillon-Robles, A., Calmus, T., Maury, R.C., Bellon, H., Cotten, J., Bourgois, J., and Michaud, F., 2002, Geochemical diversity of Miocene volcanism in southern Baja California, Mexico: Implication of mantle and crustal sources during the opening of an asthenospheric window: The Journal of Geology, v. 110, p. 627–648, doi:10.1086/342735.

Bigioggero, B., Chiesa, S., Zanchi, A., Montrasio, A., and Vezzoli, L., 1995, The Cerro Mencenares volcanic center, Baja California Sur; source and tectonic control on post-subduction magmatism within the Gulf Rift: Geological Society of America Bulletin, v. 107, p. 1108–1122, doi:10.1130/0016-7606(1995)107<1108:TCMVCB>2.3.CO;2.

Biswas, S., Coutand, I., Grujic, D., Hager, C., Stockli, D., and Grasemann, B., 2007, Exhumation and uplift of the Shillong Plateau and its influence on the eastern Himalayas: New constraints from apatite and zircon (U-Th-[Sm])/He and apatite fission track analyses: Tectonics, v. 26, TC6013, doi:10.1029/2007TC002125.

Blondes, M.S., Reiners, P.W., Edwards, B.R., and Biscontini, A., 2007, Dating young basalt eruptions by (U-Th)/He on xenolithic zircons: Geology, v. 35, p. 17–20, doi:10.1130/G22956A.1.

Bryan, S.E., and Ernst, R.E., 2008, Revised definition of large igneous provinces (LIPs): Earth-Science Reviews, v. 86, p. 175–202, doi:10.1016/j.earscirev.2007.08.008.

Calmus, T., Pallares, C., Maury, R.C., Aguillon-Robles, A., Bellon, H., Benoit, M., and Michaud, F., 2011, Volcanic markers of the post-subduction evolution of Baja California and Sonora, Mexico: Slab tearing versus lithospheric rupture of the Gulf of California: Pure and Applied Geophysics, v. 168, no. 8–9, p. 1303–1330.

Capra, L., Macias, J.L., Espindola, J.M., and Siebe, C., 1998, Holocene Plinian eruption of La Virgen Volcano, Baja California, Mexico: Journal of Volcanology and Geothermal Research, v. 80, p. 239–266, doi:10.1016/S0377-0273(97)00049-8.

Castillo, P.R., 2008, Origin of the adakite–high-Nb basalt association and its implications for postsubduction magmatism in Baja California, Mexico: Geological Society of America Bulletin, v. 120, p. 451–462, doi:10.1130/B26166.1.

Castillo, P.R., Hawkins, J.W., Lonsdale, P.F., Hilton, D.R., Shaw, A.M., and Glascock, M.D., 2002, Petrology of Alarcon Rise lavas, Gulf of California: Nascent intracontinental ocean crust: Journal of Geophysical Research–Solid Earth, v. 107, no. B10, 2222, doi:10.1029/2001JB000666.

Cheng, H., Edwards, R.L., Hoff, J., Gallup, C.D., Richards, D.A., and Asmerom, Y., 2000, The half-lives of uranium-234 and thorium-230: Chemical Geology, v. 169, p. 17–33, doi:10.1016/S0009-2541(99)00157-6.

Einsele, G., Gieskes, J.M., Curray, J., Moore, D.M., Aguayo, E., Aubry, M.-P., Fornari, D., Guerrero, J., Kastner, M., Kelts, K., Lyle, M., Matoba, Y., Molina-Cruz, A., Niemitz, J., Rueda, J., Saunders, A., Schrader, H., Simoneit, B., and Vacquier, V., 1980, Intrusion of basaltic sills into highly porous sediments, and resulting hydrothermal activity: Nature, v. 283, no. 5746, p. 441–445, doi:10.1038/283441a0.

Elders, W.A., Rex, R.W., Meidav, T., Robinson, P.T., and Biehler, S., 1972, Crustal spreading in Southern California: Science, v. 178, no. 4056, p. 15–24, doi:10.1126/science.178.4056.15.

Farley, K.A., Wolf, R.A., and Silver, L.T., 1996, The effects of long alpha-stopping distances on (U-Th)/He ages: Geochimica et Cosmochimica Acta, v. 60, p. 4223–4229, doi:10.1016/S0016-7037(96)00193-7.

Farley, K.A., Kohn, B.P., and Pillans, B., 2002, The effects of secular disequilibrium on (U-Th)/He systematics and dating of Quaternary volcanic zircon and apatite: Earth and Planetary Science Letters, v. 201, p. 117–125, doi:10.1016/S0012-821X(02)00659-3.

Ferrari, L., Lopez-Martinez, M., Aguirre-Diaz, G., and Carrasco-Nunez, G., 1999, Space-time patterns of Cenozoic arc volcanism in central Mexico: From the Sierra Madre Occidental to the Mexican volcanic belt: Geology, v. 27, p. 303–306, doi:10.1130/0091-7613(1999)027<0303:STPOCA>2.3.CO;2.

Ferry, J.M., and Watson, E.B., 2007, New thermodynamic models and revised calibrations for the Ti-in-zircon and Zr-in-rutile thermometers: Contributions to Mineralogy and Petrology, v. 154, p. 429–437, doi:10.1007/s00410-007-0201-0.

France, L., Koepke, J., Ildefonse, B., Cichy, S.B., and Deschamps, F., 2010, Hydrous partial melting in the sheeted dike complex at fast spreading ridges: Experimental and natural observations: Contributions to Mineralogy and Petrology, v. 160, p. 683–704, doi:10.1007/s00410-010-0502-6.

Friedman, I., and Obradovich, J., 1981, Obsidian hydration dating of volcanic events: Quaternary Research, v. 16, p. 37–47, doi:10.1016/0033-5894(81)90126-5.

Fuis, G.S., Mooney, W.D., Healy, J.H., McMechan, G.A., and Lutter, W.J., 1984, A seismic refraction survey of the Imperial Valley region, California: Journal of Geophysical Research, ser. B, v. 89, p. 1165–1189, doi:10.1029/JB089iB02p01165.

Gibson, S.A., Thompson, R.N., Weska, R.K., Dickin, A.P., and Leonardos, O.H., 1997, Late Cretaceous rift-related upwelling and melting of the Trindade starting mantle plume head beneath western Brazil: Contributions to Mineralogy and Petrology, v. 126, no. 3, p. 303–314, doi:10.1007/s004100050252.

González-Escobar, M., Aguilar-Campos, C., Suarez-Vidal, F., and Martin-Barajas, A., 2009, Geometry of the Wagner basin, upper Gulf of California based on seismic reflections: International Geology Review, v. 51, no. 2, p. 133–144, doi:10.1080/00206810802615124.

Gonzalez-Escobar, M., Suarez-Vidal, F., Hernandez-Perez, J.A., and Martin-Barajas, A., 2010, Seismic reflection–based evidence of a transfer zone between the Wagner and Consag basins: Implications for defining the structural geometry of the northern Gulf of California: Geo-Marine Letters, v. 30, no. 6, p. 575–584, doi:10.1007/s00367-010-0204-0.

Grimes, C.B., John, B.E., Kelemen, P.B., Mazdab, F.K., Wooden, J.L., Cheadle, M.J., Hanghoj, K., and Schwartz, J.J., 2007, Trace element chemistry of zircons from oceanic crust; a method for distinguishing detrital zircon provenance: Geology, v. 35, no. 7, p. 643–646, doi:10.1130/G23603A.1.

Grimes, C.B., Ushikubo, T., John, B.E., and Valley, J.W., 2011, Uniformly mantle-like $\delta^{18}O$ in zircons from oceanic plagiogranites and gabbros: Contributions to Mineralogy and Petrology, v. 161, p. 13–33, doi:10.1007/s00410-010-0519-x.

Grove, M., Jacobson, C.E., Barth, A.P., and Vucic, A., 2003, Temporal and spatial trends of Late Cretaceous–early Tertiary underplating of Pelona and related schist beneath Southern California and southwestern Arizona, *in* Johnson, S.E., Paterson, S.R., Fletcher, J.M., Girty, G.H., Kimbrough, D.L., and Martín-Barajas, A., eds., Tectonic Evolution of Northwestern México and the Southwestern USA: Geological Society of America Special Paper 374, p. 381–406.

Hausback, B.P., 1984, Cenozoic volcanic and tectonic evolution of Baja California Sur, *in* Frizzell, V., ed., Geology of the Baja California Peninsula: Society of Economic Paleontologists and Mineralogists (SEPM), Pacific Section, Bakersfield, California, p. 219–236.

Heizler, M.T., and Harrison, T.M., 1991, The heating duration and provenance age of rocks in the Salton Sea geothermal field, Southern California: Journal of Volcanology and Geothermal Research, v. 46, p. 73–97, doi:10.1016/0377-0273(91)90077-D.

Herzig, C.T., 1990, Geochemistry of igneous rocks from the Cerro Prieto geothermal field, northern Baja California, Mexico: Journal of Volcanology and Geothermal Research, v. 42, p. 261–271, doi:10.1016/0377-0273(90)90003-X.

Herzig, C.T., and Elders, W.A., 1988, Nature and significance of igneous rocks cored in the state 2–14 research borehole, Salton Sea Scientific Drilling Project, California: Journal of Geophysical Research–Solid Earth and Planets, v. 93, no. B11, p. 13,069–13,080, doi:10.1029/JB093iB11p13069.

Herzig, C.T., and Jacobs, D.C., 1994, Cenozoic volcanism and two-stage extension in the Salton Trough, Southern California and northern Baja California: Geology, v. 22, p. 991–994, doi:10.1130/0091-7613(1994)022<0991:CVATSE>2.3.CO;2.

Hurtado-Brito, J.C., 2012, El Registro Volcánico en las Cuencas Rift del Norte del Golfo de California a Partir de Sísmica de Reflexión [Master's thesis]: Ensenada, Mexico, CICESE, 100 p.

Jaffey, A.H., Flynn, K.F., Glendenin, L.E., Bentley, W.C., and Essling, A.M., 1971, Precision measurement of half-lives and specific activities of ^{235}U and ^{238}U: Physical Review C: Nuclear Physics, v. 4, p. 1889–1906, doi:10.1103/PhysRevC.4.1889.

Kasameyer, P.W., and Hearst, J.R., 1988, Borehole gravity measurements in the Salton Sea Scientific Drilling Project well state 2–14: Journal of Geophysical Research–Solid Earth and Planets, v. 93, p. 13,037–13,045, doi:10.1029/JB093iB11p13037.

Kelley, V.C., and Soske, J.L., 1936, Origin of the Salton volcanic domes, Salton Sea, California: The Journal of Geology, v. 44, p. 496–509, doi:10.1086/624444.

Krogh, T.E., 1973, A low-contamination method for hydrothermal decomposition of zircon and extraction of U and Pb for isotopic age determinations: Geochimica et Cosmochimica Acta, v. 37, p. 485–494.

Liu, Y.S., Hu, Z.C., Zong, K.Q., Gao, C.G., Gao, S., Xu, J.A., and Chen, H.H., 2010, Reappraisement and refinement of zircon U-Pb isotope and trace element analyses by LA-ICP-MS: Chinese Science Bulletin, v. 55, no. 15, p. 1535–1546, doi:10.1007/s11434-010-3052-4.

Lizarralde, D., Axen, G.J., Brown, H.E., Fletcher, J.M., Gonzalez-Fernandez, A., Harding, A.J., Holbrook, W.S., Kent, G.M., Paramo, P., Sutherland, F., and Umhoefer, P.J., 2007, Variation in styles of rifting in the Gulf of California: Nature, v. 448, p. 466–469, doi:10.1038/nature06035.

Lonsdale, P.F., 1989, Geology and tectonic history of the Gulf of California, *in* Winterer, E.L., Hussong, D.M., and Decker, R.W., eds., The Eastern Pacific Ocean and Hawaii: Boulder, Colorado, Geological Society of America, The Geology of North America, v. N, p. 499–521.

Martín, A., Fletcher, J.M., Lopez-Martinez, M., and Mendoza-Borunda, R., 2000, Waning Miocene subduction and arc volcanism in Baja California: The San Luis Gonzaga volcanic field: Tectonophysics, v. 318, p. 27–51, doi:10.1016/S0040-1951(99)00305-4.

Martín, A., Hurtado, J.C., Cañon, E., Weber, B., and Schmitt, A.K., 2013, Extent and composition of the new crust beneath rift basins in the northern Gulf of California: Geological Society of America Abstracts with Programs, v. 45, no. 6, p. 22.

Martin, E., and Sigmarsson, O., 2007, Crustal thermal state and origin of silicic magma in Iceland: The case of Torfajokull, Ljosufjoll and Snaefellsjokull volcanoes: Contributions to Mineralogy and Petrology, v. 153, p. 593–605, doi:10.1007/s00410-006-0165-5.

Martín-Barajas, A., and Weber, B., 2003, Petrology of Plio-Pleistocene volcanic rocks in the northern Gulf of California rift system; insights into crustal composition: Geological Society of America Abstracts with Programs, v. 35, no. 4, p. 28–29.

Martín-Barajas, A., Stock, J.M., Layer, P., Hausback, B., Renne, P., and Lopez-Martinez, M., 1995, Arc-rift transition volcanism in the Puertecitos Volcanic Province, northeastern Baja-California, Mexico: Geological Society of America Bulletin, v. 107, p. 407–424, doi:10.1130/0016-7606(1995)107<0407:ARTVIT>2.3.CO;2.

Martín-Barajas, A., Weber, B., Schmitt, A.K., and Lonsdale, P., 2008, Recent rift volcanism in the northern Gulf of California and the Salton Trough: Why a preponderance of evolved magmas?: San Francisco, American Geophysical Union, Fall Meeting, abstract T11A–1841.

McDowell, S.D., and Elders, W.A., 1980, Authigenic layer silicate minerals in borehole Elmore-1, Salton Sea geothermal field, California, USA: Contributions to Mineralogy and Petrology, v. 74, p. 293–310, doi:10.1007/BF00371699.

McKibben, M.A., Andes, J.P., and Williams, A.E., 1988, Active ore formation at a brine interface in metamorphosed deltaic lacustrine sediments; the Salton Sea geothermal system, California: Economic Geology and the Bulletin of the Society of Economic Geologists, v. 83, no. 3, p. 511–523, doi:10.2113/gsecongeo.83.3.511.

Monteleone, B.D., Baldwin, S.L., Webb, L.E., Fitzgerald, P.G., Grove, M., and Schmitt, A.K., 2007, Late Miocene–Pliocene eclogite facies metamorphism, D'Entrecasteaux Islands, SE Papua New Guinea: Journal of Metamorphic Geology, v. 25, p. 245–265, doi:10.1111/j.1525-1314.2006.00685.x.

Mora-Klepeis, G., and McDowell, F.W., 2004, Late Miocene calc-alkalic volcanism in northwestern Mexico: An expression of rift or subduction-related magmatism?: Journal of South American Earth Sciences, v. 17, p. 297–310, doi:10.1016/j.jsames.2004.08.001.

Negrete-Aranda, R., and Canon-Tapia, E., 2008, Post-subduction volcanism in the Baja California Peninsula, Mexico: The effects of tectonic reconfiguration in volcanic systems: Lithos, v. 102, p. 392–414, doi:10.1016/j.lithos.2007.08.013.

Nicholls, I.A., 1974, Direct fusion method of preparing silicate rock glasses for energy-dispersive electron-microprobe analysis: Chemical Geology, v. 14, p. 151–157, doi:10.1016/0009-2541(74)90124-7.

Niu, Y.L., Collerson, K.D., Batiza, R., Wendt, J.I., and Regelous, M., 1999, Origin of enriched-type mid-ocean ridge basalt at ridges far from mantle plumes: The East Pacific Rise at 11 degrees 20′N: Journal of Geophysical Research–Solid Earth, v. 104, p. 7067–7087, doi:10.1029/1998JB900037.

Oskin, M., and Stock, J., 2003, Pacific–North America plate motion and opening of the Upper Delfin basin, northern Gulf of California, Mexico: Geological Society of America Bulletin, v. 115, no. 10, p. 1173–1190, doi:10.1130/B25154.1.

Pacheco, M., Martín-Barajas, A., Elders, W., Espinosa-Cardeña, J.M., Helenes, J., and Segura, A., 2006, Stratigraphy and structure of the Altar basin of NW Sonora: Implications for the history of the Colorado River delta and the Salton Trough: Revista Mexicana de Ciencias Geológicas, v. 23, no. 1, p. 1–22.

Parsons, T., and McCarthy, J., 1996, Crustal and upper mantle velocity structure of the Salton Trough, southeast California: Tectonics, v. 15, no. 2, p. 456–471, doi:10.1029/95TC02616.

Paz-Moreno, F.A., and Demant, A., 1999, The Recent Isla San Luis volcanic centre: Petrology of a rift-related volcanic suite in the northern Gulf of California, Mexico: Journal of Volcanology and Geothermal Research, v. 93, p. 31–52, doi:10.1016/S0377-0273(99)00083-9.

Pearce, N.J.G., Perkins, W.T., Westgate, J.A., Gorton, M.P., Jackson, S.E., Neal, C.R., and Chenery, S.P., 1997, A compilation of new and published major and trace element data for NIST SRM 610 and NIST SRM 612 glass reference materials: Geostandards Newsletter—The Journal of Geostandards and Geoanalysis, v. 21, no. 1, p. 115–144, doi:10.1111/j.1751-908X.1997.tb00538.x.

Persaud, P., Stock, J.M., Steckler, M.S., Martín-Barajas, A., Diebold, J.B., González-Fernández, A., and Mountain, G.S., 2003, Active deformation and shallow structure of the Wagner, Consag, and Delfín Basins, northern Gulf of California, Mexico: Journal of Geophysical Research: Solid Earth, v. 108, no. B7, 2355, doi:10.1029/2002JB001937.

Reed, M.J., Wright, R., and Richards, R.G., 1984, Relationship between volcanism and hydrothermal activity at Cerro Prieto, Mexico: Transactions, Geothermal Resources Council, v. 8, p. 217–221.

Reid, M.R., Coath, C.D., Harrison, T.M., and McKeegan, K.D., 1997, Prolonged residence times for the youngest rhyolites associated with Long Valley Caldera; ^{230}Th-^{238}U ion microprobe dating of young zircons: Earth and Planetary Science Letters, v. 150, p. 27–39, doi:10.1016/S0012-821X(97)00077-0.

Robinson, P.T., Elders, W.A., and Muffler, L.J.P., 1976, Quaternary volcanism in Salton Sea geothermal field, Imperial Valley, California: Geological Society of America Bulletin, v. 87, p. 347–360, doi:10.1130/0016-7606(1976)87<347:QVITSS>2.0.CO;2.

Sawlan, M.G., 1991, Magmatic evolution of the Gulf of California rift, *in* Dauphin, J.P., and Simoneit, B.R., eds., The Gulf and Peninsular Province of the Californias: American Association of Petroleum Geologists Memoir 47, p. 301–369.

Schmitt, A.K., and Hulen, J.B., 2008, Buried rhyolites within the active, high-temperature Salton Sea geothermal system: Journal of Volcanology and Geothermal Research, v. 178, p. 708–718, doi:10.1016/j.jvolgeores.2008.09.001.

Schmitt, A.K., and Vazquez, J.A., 2006, Alteration and remelting of nascent oceanic crust during continental rupture: Evidence from zircon geochemistry of rhyolites and xenoliths from the Salton Trough, California: Earth and Planetary Science Letters, v. 252, p. 260–274, doi:10.1016/j.epsl.2006.09.041.

Schmitt, A.K., Grove, M., Harrison, T.M., Lovera, O., Hulen, J., and Walters, M., 2003, The Geysers–Cobb Mountain magma system, California (Part 1): U-Pb zircon ages of volcanic rocks, conditions of zircon crystallization and magma residence times: Geochimica et Cosmochimica Acta, v. 67, p. 3423–3442, doi:10.1016/S0016-7037(03)00140-6.

Schmitt, A.K., Stockli, D.F., and Hausback, B.P., 2006, Eruption and magma crystallization ages of Las Tres Virgenes (Baja California) constrained by combined Th-230/U-238 and (U-Th)/He dating of zircon: Journal of Volcanology and Geothermal Research, v. 158, p. 281–295, doi:10.1016/j.jvolgeores.2006.07.005.

Schmitt, A.K., Stockli, D.F., Niedermann, S., Lovera, O.M., and Hausback, B.P., 2010, Eruption ages of Las Tres Vírgenes volcano (Baja California): A tale of two helium isotopes: Quaternary Geochronology, v. 5, no. 5, p. 503–511.

Schmitt, A.K., Perfit, M.R., Rubin, K.H., Stockli, D.F., Smith, M.C., Cotsonika, L.A., Zellmer, G.F., Ridley, W.I., and Lovera, O.M., 2011, Rapid cooling rates at an active mid-ocean ridge from zircon thermochronology: Earth and Planetary Science Letters, v. 302, p. 349–358, doi:10.1016/j.epsl.2010.12.022.

Schmitt, A.K., Martín, A., Stockli, D.F., Farley, K.A., and Lovera, O.M., 2013, (U-Th)/He zircon and archaeological ages for a late prehistoric eruption in the Salton Trough (California): Geology, v. 41, p. 7–10, doi:10.1130/G33634.1.

Shen, C.-C., Lawrence Edwards, R., Cheng, H., Dorale, J.A., Thomas, R.B., Bradley Moran, S., Weinstein, S.E., and Edmonds, H.N., 2002, Uranium and thorium isotopic and concentration measurements by magnetic sector inductively coupled plasma mass spectrometry: Chemical Geology, v. 185, p. 165–178, doi:10.1016/S0009-2541(01)00404-1.

Shen, C.-C., Cheng, H., Edwards, R.L., Moran, S.B., Edmonds, H.N., Hoff, J.A., and Thomas, R.B., 2003, Measurement of attogram quantities of ^{231}Pa in dissolved and particulate fractions of seawater by isotope dilution thermal ionization mass spectroscopy: Analytical Chemistry, v. 75, p. 1075–1079, doi:10.1021/ac026247r.

Shen, C.-C., Wu, C.-C., Cheng, H., Edwards, R.L., Hsieh, Y.-T., Gallet, S., Chang, C.-C., Li, T.-Y., Lam, D.D., Kano, A., Hori, M., and Spötl, C., 2012, High-precision and high-resolution carbonate ^{230}Th dating by MC-ICP-MS with SEM protocols: Geochimica et Cosmochimica Acta, v. 99, p. 71–86, doi:10.1016/j.gca.2012.09.018.

Thy, P., Beard, J.S., and Lofgren, G.E., 1990, Experimental constraints on the origin of Icelandic rhyolites: The Journal of Geology, v. 98, p. 417–421, doi:10.1086/629413.

Till, C.B., Gans, P.B., Spera, F.J., MacMillan, I., and Blair, K.D., 2009, Perils of petrotectonic modeling: A view from southern Sonora, Mexico: Journal of Volcanology and Geothermal Research, v. 186, no. 3–4, p. 160–168, doi:10.1016/j.jvolgeores.2009.06.014.

Trail, C.B., Mojzsis, S.J., Harrison, T.M., Schmitt, A.K., Watson, E.B., and Young, E.D., 2007, Constraints on Hadean zircon protoliths from oxygen isotopes, Ti-thermometry, and rare earth elements: Geochemistry Geophysics Geosystems, v. 8, Q06014, doi:10.1029/2006GC001449.

Trail, D., Bindeman, I.N., Watson, E.B., and Schmitt, A.K., 2009, Experimental calibration of oxygen isotope fractionation between quartz and zircon: Geochimica et Cosmochimica Acta, v. 73, p. 7110–7126, doi:10.1016/j.gca.2009.08.024.

Umhoefer, P.J., Dorsey, R.J., Willsey, S., Mayer, L., and Renne, P.R., 2001, Stratigraphy and geochronology of the Comondú Group near Loreto, Baja California Sur, Mexico: Sedimentary Geology, v. 144, p. 125–147, doi:10.1016/S0037-0738(01)00138-5.

Valley, J.W., 2003, Oxygen isotopes in zircon: Reviews in Mineralogy and Geochemistry, v. 53, p. 343–385, doi:10.2113/0530343.

Vazquez, J.A., and Reid, M.R., 2004, Probing the accumulation history of the voluminous Toba magma: Science, v. 305, p. 991–994, doi:10.1126/science.1096994.

Vidal-Solano, J.R., Demant, A., Moreno, F.A.P., Lapierre, H., Ortega-Rivera, M.A., and Lee, J.K.W., 2008, Insights into the tectonomagmatic evolution of NW Mexico: Geochronology and geochemistry of the Miocene volcanic rocks from the Pinacate area, Sonora: Geological Society of America Bulletin, v. 120, p. 691–708, doi:10.1130/B26053.1.

Wanless, V.D., Perfit, M.R., Ridley, W.I., and Klein, E., 2010, Dacite petrogenesis on mid-ocean ridges: Evidence for oceanic crustal melting and assimilation: Journal of Petrology, v. 51, p. 2377–2410, doi:10.1093/petrology/egq056.

Wiedenbeck, M., Hanchar, J.M., Peck, W.H., Sylvester, P., Valley, J., Whitehouse, M., Kronz, A., Morishita, Y., Nasdala, L., Fiebig, J., Franchi, I., Girard, J.P., Greenwood, R.C., Hinton, R., Kita, N., Mason, P.R.D., Norman, M., Ogasawara, M., Piccoli, P.M., Rhede, D., Satoh, H., Schulz-Dobrick, B., Skar, O., Spicuzza, M.J., Terada, K., Tindle, A., Togashi, S., Vennemann, T., Xie, Q., and Zheng, Y.F., 2004, Further characterisation of the 91500 zircon crystal: Geostandards and Geoanalytical Research, v. 28, p. 9–39, doi:10.1111/j.1751-908X.2004.tb01041.x.

Wilson, S.A., 1997, Data Compilation for USGS Reference Material BHVO-2, Hawaiian Basalt: U.S. Geological Survey Open-File Report: http://crustal.usgs.gov/geochemical_reference_standards/basaltbhvo2.html (accessed 28 July 2012).

Science Editor: Nancy Riggs
Associate Editor: Brian McConnell

Manuscript Received 28 August 2012
Revised Manuscript Received 25 May 2013
Manuscript Accepted 7 August 2013

Printed in the USA